Potent tetrahydroquinolone eliminates apicomplexan parasites

Martin McPhillie[1], Ying Zhou[2], Mark Hickman[3], James Gordon[1], Christopher R. Weber[2], Qigui Li[3], Patty Lee[3], Kangsa Amporndanai[4], Rachel Johnson[1], Heather Darby[1], Stuart Woods[5], Zhuhong Li[6], Richard S. Priestley[7], Kurt Ristroph[8], Scott B. Biering[2], KAMAL EL BISSATI[2], Seungmin ". Hwang[2], Farida E. Hakim[9], Sarah Dovgin[2], Joseph D. Lykins[2], Lucy Roberts[5], Kerrie Hargrave[5], Hua Cong[2], Anthony P. Sinai[10], Stephen P. Muench[1], Jitender Dubey[11], Robert Prud'homme[8], Hernan A. Lorenzi[12], Giancarlo A. Biagini[7], Silvia N. Moreno[6*], Craig W. Roberts[5], Svetlana Atonyuk[4*], Colin Fishwick[1*], Rima McLeod[2*]

[1]University of Leeds, United Kingdom, [2]University of Chicago, United States, [3]Walter Reed Army Institute of Research, United States, [4]University of Liverpool, United Kingdom, [5]University of Strathclyde, United Kingdom, [6]University of Georgia, United States, [7]Liverpool School of Tropical Medicine, United Kingdom, [8]Princeton University, United States, [9]University of Chicago Medicine, United States, [10]University of Kentucky, United States, [11]United States Department of Agriculture (USDA), United States, [12]J. Craig Venter Institute (La Jolla), United States

Submitted to Journal:
Frontiers in Cellular and Infection Microbiology

Specialty Section:
Parasite and Host

Article type:
Original Research Article

Manuscript ID:
536546

Received on:
20 Feb 2020

Revised on:
09 Apr 2020

Frontiers website link:
www.frontiersin.org

Conflict of interest statement

The authors declare that the research was conducted in the absence of any commercial or financial relationships that could be construed as a potential conflict of interest

Author contribution statement

Conception and Design. Overall: MMc, RMc, MH, HL, SNM, CWF, CWR, SPM, GB, SA, KR, RP, LY; Subparts of manuscript: all authors.
Performed Experiments and/or analyzed data. All authors.
Wrote manuscript. Overall: MMc, RMc, MH, HL; Subparts of manuscript: all authors.
Reviewed/Edited Manuscript in final form: All Authors

Keywords

Toxoplasma gondii, Plasmodium falciparum, Plasmodium bergheii, cytochrome b/c Qi domain, inhibitor, SAR, potent lead compound, JAG21, tetrahyroquinolone, tachyzoite, Bradyzoite, Atovaquone, Qo domain, Synergy, admet, co-crystallography, co-cryo-electronmicroscopy, enzyme activity, Causal prophylaxis, Radical cure, RPS13D, Plasmodium cynomogoli hypnozoite single cell RNA sequencing, Transcriptomics, stasis form, Tafenoquine, companion compounds, stable nanoformulation, Effective treatment

Abstract

Word count: 150

Apicomplexan infections cause substantial morbidity and mortality, worldwide. New, improved therapies are needed. Herein, we create a next generation anti-apicomplexan lead compound, JAG21, a tetrahydroquinolone, with increased sp3-character to improve parasite selectivity. Relative to other cytochromeb inhibitors, JAG21 has improved solubility and ADMET properties, without need for pro-drug. JAG21 significantly reduces Toxoplasma gondii tachyzoites and encysted bradyzoites in vitro, and in primary and established chronic infections in vivo. Moreover, JAG21 treatment leads to 100% survival. Further, JAG21 is efficacious against drug-resistant Plasmodium falciparum in vitro. Causal prophylaxis and radical cure are achieved after P. berghei sporozoite infection with oral administration of a single dose (2.5mg/kg) or three days treatment at reduced dose (0.625mg/kg/day), eliminating parasitemia and leading to 100% survival. Enzymatic, binding, and co-crystallography/pharmacophore studies demonstrate selectivity for apicomplexan relative to mammalian enzymes. JAG21 has significant promise as a pre-clinical candidate for prevention, treatment and cure of toxoplasmosis and malaria.

Contribution to the field

We find that JAG21 is effective against actively replicating T.gondii tachyzoites, and previously untreatable chronic encysted bradyzoite brain stage in vitro , and in mice. We demonstrate JAG21's synergy with a cytochrome b/c qo inhibitor atovaquone against tachyzoites. JAG21 also is effective in vitro against drug susceptible and known drug resistant forms of P. falciparum. JAG21 is effective as causal prophylaxis and definitive cure in a single oral dose of 2.5mg/kg for P.bergheii murine malaria. JAG21 inhibits both Toxoplasma and Plasmodia cytochrome b qi and has ADMET properties suitable to become a medicine for people. We prove JAG21's mechanism of action, using enzymology, binding assays, co crystallography and co cryo-electron microscopy. We discover how it might be further improved, if this were needed. We demonstrate safety and efficacy against T. gondii tachyzoites and previously untreatable latent bradyzoites, the form of the organism that is present in the brain of 2 billion people worldwide, lifelong, and against plasmodia. JAG21 treatment of conditional mutant deltaRPS13 and transcriptomics define a metabolically quiescent "persister","stasis" state that is reversible even after substantial periods of dormancy,. This contributes to conceptual and functional understanding of both Plasmodia and Toxoplasma infections and molecular mechanisms whereby "persisters" might be eliminated. Moving toward addressing this question, optimizing treatment , and identifying co-administered companion compounds that may lead to definitive cure for human infections, we created a stable nanoformulated JAG21. Using this new formulation, we determined that oral administration of JAG21 reduces parasite burden after infection of mice with a highly virulent strain of T.gondii.

Funding statement

This work was supported by NIAID NIH DMID U01 AI082180 and the National Institute of Diabetes and Digestive and Kidney Diseases (NIDDK) Grant #5T35DK062719-28 to FE. This was also supported by National Institutes of Health (NIH) contract number HHNS272200900007C, NIH. National Institute of Allergy and Infectious Diseases of the National Institutes of Health (NIAID) award numbers R01AI071319(NIAID) and R01AI027530 (NIAID) ;NIAID contract Number HHNS272200900007C; MIAID award number

U19AI110819: NIAID award number U01 AI077887(NIAID) and Defense Threat Reduction Agency award number 13-C-0055, and Department of Defense award numbers W911NF-09-D0001 and W911SR-07-C0101. We thank and gratefully also acknowledge the support of the Cornwell Mann family, the Ramirez, Musillami, Quinn, Rosenthal, Greenberg, Morel, Rooney and Engel families, Taking out Toxo, and The Toxoplasmosis Research Institute. The work also was supported by the Bill and Melinda Gates Foundation (BMGF, OPP1150755). This material is based upon work supported by the National Science Foundation Graduate Research Fellowship under Grant No. #DGE-1656466 awarded to K.D.R.

Ethics statements

Studies involving animal subjects

Generated Statement: The animal study was reviewed and approved by This study was carried out in accordance with regulations of The University of Chicago IACUC and IBC and of The Home Office of the UK Government under the Animals [Scientific Procedures] Act 1986. All work in the UK with mice was covered by License PPL60/4568, Treatment and Prevention of Toxoplasmosis with approval by the University of Strathclyde ethical review board. .

Studies involving human subjects

Generated Statement: No human studies are presented in this manuscript.

Inclusion of identifiable human data

Generated Statement: No potentially identifiable human images or data is presented in this study.

Data availability statement

Generated Statement: This manuscript contains previously unpublished data. The name of the repository and accession number(s) are not available.

Potent tetrahydroquinolone eliminates apicomplexan parasites

Martin McPhillie[1,+] , Ying Zhou[2,+], Mark Hickman[3,+,++], James Gordon[1,++,+], Christopher R. Weber[2,+], Qigui Li[3], Patty Lee[3], Kangsa Amporndanai[4], Rachel Johnson[1,++], Heather Darby[1], Stuart Woods[5], Zhu-hong Li[6], Richard S. Priestley[7], Kurt Ristroph[8], Scott Biering[2,++] , Kamal El Bissati[2], Seungmin Hwang[2++], Farida Esaa Hakim [2], Sarah Dovgin[2,++] Joseph Lykins[2,++], Lucy Roberts[5,++], Kerrie Hargrave[5,++], Hua Cong[1,++], Anthony P. Sinai[9], Stephen P. Muench[1], Jitender Dubey[10] , Robert Prud'homme [8], Hernan Lorenzi[11], Giancarlo A Biagini[7], Silvia N. Moreno[6,*] Craig Roberts[5], Svetlana Atonyuk[4,*], Colin Fishwick[1,*], Rima McLeod[2,*]

[1]The University of Leeds, Leeds, UK

[2]The University of Chicago, Chicago, USA

[3]Walter Reed Army Institute of Research. USA

[4]The University of Liverpool, Liverpool, UK

[5]The University of Strathclyde, Glasgow Scotland, UK

[6]The University of Georgia, Athens Georgia, USA

[7]The Liverpool School of Tropical Medicine, Liverpool, UK

[8]Princeton University, Princeton, New Jersey, USA

[9]The University of Kentucky College of Medicine, Lexington, USA

[10]USDA, ARS, APDL, Beltsville, Maryland, USA

[11]J Craig Venter Institute, Rockville, Maryland, USA

[+]These authors contributed equally to this work

[*]To whom Correspondence should be addressed

[++]Currently at : Charles River UK(JG); Fort Dietrick (MH); University of California at Berkeley(SB); Monash University, Australia(RJ); VIR Biotechnology. (SH); Case Western Reserve University (SD); Medical College of Virginia (JL), Shandong University(HC); University of Glasgow (KH)

Word count: 11,988 original (with edits suggested 13, 643)
Figures 7
In Supplement: 2 Supplemental tables and supplemental text 2 supplental figures

ABSTRACT

Apicomplexan infections cause substantial morbidity and mortality, worldwide. New, improved therapies are needed. Herein, we create a next generation anti-apicomplexan lead compound, JAG21, a tetrahydroquinolone, with increased sp3-character to improve parasite selectivity. Relative to other cytochrome*b* inhibitors, JAG21 has improved solubility and ADMET properties, without need for pro-drug. JAG21 significantly reduces *Toxoplasma gondii* tachyzoites and encysted bradyzoites *in vitro,* and in primary and established chronic murine infections. Moreover, JAG21 treatment leads to 100% survival. Further, JAG21 is efficacious against drug-resistant *Plasmodium falciparum in vitro.* Causal prophylaxis and radical cure are achieved after *P. berghei* sporozoite infection with oral administration of a single dose (2.5mg/kg) or three days treatment at reduced dose (0.625mg/kg/day), eliminating parasitemia and leading to 100% survival. Enzymatic, binding, and co-crystallography/pharmacophore studies demonstrate selectivity for apicomplexan relative to mammalian enzymes. JAG21 has significant promise as a pre-clinical candidate for prevention, treatment and cure of toxoplasmosis and malaria.

Keywords*: Toxoplasma gondii, Plasmodium falciparum, Plasmodium bergheii,*, cytochrome b/c Qi domain, inhibitor, SAR, potent lead compound, JAG21, tetrahyroquinolone, tachyzoite, bradyzoite, atovaquone, Qo domain, synergy, ADMET, co-crystallography, co-cryo-electronmicroscopy, enzyme activity, causal prophylaxis, radical cure, RPS13Δ, *Plasmodium cynomogoli hypnozoite single cell RNA sequencing, transcriptomics, stasis form, tafenoquine, companion compounds, stable* nanoformulation, effective treatment

INTRODUCTION

Malaria results in the death of ~0.5 million children a year, with drug resistance impacting the usefulness of successive generations of new medicines ((www.who.int/malaria/publications/world-malaria-report-2017/en/). The related apicomplexan parasite, *Toxoplasma gondii,* is the most frequent parasitic infection of humans in the world. It plays a significant role in food-born associated death in the USA, destruction of the human retina, and death and illness from recrudescent disease in the immune compromised or immunologically immature (McLeod, Boyer, 2018). It has been estimated that there are 1.9 million new cases of this congenital *T. gondii* infection globally over a ten year period, causing 12 million disability adjusted life years (Torgerson and Mastroiacovo, 2013) from damage to the fetal brain and eye. Toxoplasmosis is an often neglected, untreated or mistreated disease. There are approximately 2 billion people throughout the world who have this parasite in their brain lifelong, some with known, severe, adverse consequences (Delair et al, 2011; Lykins et al, 2016; Wallon et al, 2013). There are possible additional, harmful effects for a substantial number of chronically infected people as this parasite modulates signature pathways of neurodegeneration, motor diseases, epilepsy, and malignancies (Ngo et al, 2017). No medicine eliminates this chronic, encysted form of the parasite. New and improved medicines are greatly needed to cure *Toxoplasma* and Plasmodia infections. These parasites often share the same molecular targets for medicines due to a relatively close, apicomplexan, phylogenetic relationship (McPhillie et al, 2016).

Thus, medicine development for each of these parasites can inform development of medicines that benefit treating the other (Muench et al 2007; Fomovska et al, 2012).

One such shared molecular target is the mitochondrial cytochrome *bc1* complex that is important for the survival of apicomplexan parasites such as Plasmodia and *T gondii*. Cytochrome *b* is a subunit of the cytochrome bc_1 complex, an inner mitochondrial membrane protein that is part of the electron transport chain. Activity of this complex is integral to oxidative phosphorylation and generation of ATP (Vercesi et al, 1998). Cytochrome *b* activity appears to be necessary for the replication and persistence of the parasite (McPhillie et al 2016), and is the site of action of atovaquone (McPhillie et al, 2016). Cytochrome *b* is the target for quinolone-based compounds, but, significant problems with solubility and toxicity have been noted with earlier cytochrome *b* inhibitors. In an attempt to design novel quinolone-like inhibitors with improved solubility, and lower toxicity, compared to known compounds in the literature, we synthesized a series of tetrahydroquinolinones (THQs). Our preliminary efforts were described in McPhillie *et al* (2016). We reasoned that the increased 'sp3' character of the THQs (i.e. moving from rod-like to sphere-like 3D space) could provide the required improvement in solubility that would allow for optimal pharmacokinetic properties. Molecules with an increased percentage of 'sp3 character' tend to be more three-dimensional, than their planar ('sp2-rich') counterparts. The terms 'sp2' and 'sp3' refer to the shape of their hybridised atomic orbitals, which have trigonal planar and tetrahedral geometries respectively. Flat aromatic rings ('sp2-rich') are ubiquitous in drug discovery campaigns, but molecules with more 'sp3 character' are often more specific for their protein target and can have better physicochemical properties. Further, we reasoned that the larger binding pocket in the parasite enzymes (McPhillie et al, 2016), compared to their mammalian counterparts, would provide room for bulkier substituents to minimize effect on the human enzyme. Within this new series of compounds, we aimed to identify a mature lead compound with both anti-*Plasmodium* and anti-*T. gondii* activity.

Our work developed as follows: We recently found markedly increased expression of cytochrome *b* in the currently untreatable *T. gondii* bradyzoite life-cycle stage (McPhillie et al 2016). Thus, we set out to develop a compound that would inhibit tachyzoites, bradyzoites and three life cycle stages of even drug-resistant Plasmodia. We sought to do this without a need for a pro-drug as has been needed in other attempts to target apicomplexan cytochrome *b* (Frueh et al 2017). Our aim was to improve upon the physicochemical properties of napthoquinones and endochin-like quinolones (ELQs) targeting cytochrome *b*, including poor aqueous solubility and toxicity (McPhillie et al, 2016 ; Khan et al, 1998; Doggett et al, 2012; Capper et al, 2015; Miley et al, 2015). The intent was further to provide potential solutions for limitations of other compounds active against apicomplexan parasites (Waxman and Herbert, 1969; Caumes et al, 1995). Our concurrent crystallographic studies also enable better understanding of the interactions between ligand and the binding pocket of the Q_i site (McPhillie et al,2016).

Herein, we have identified a preclinical lead candidate based on potent and selective inhibition of *P. falciparum* and *P. berghei* and *T. gondii* cytochrome *bc1* for the treatment of malaria and toxoplasmosis. The candidate compound demonstrates high efficacy in relevant *in vitro* and *in vivo* models of the diseases, and has considerable potential for broad-spectrum use (i.e., against *T. gondii* tachyzoites and encysted bradyzoites and drug resistant Plasmodia). The data which follow present the creation and characterization of this novel, broad-spectrum, anti-apicomplexan lead compound which has promise for definitive treatment of these infections.

MATERIALS AND METHODS

Syntheses of compounds

Synthesis of tetrahydroquinolones (THQs) compounds.
The THQ compounds were synthesized at the University of Leeds as described below. 10 mM stock solutions were made with 100% Dimethyl Sulfoxide (DMSO) [Sigma Aldrich] and working concentrations were made with IMDM-C (1x, [+] glutamine, [+] 25 mM HEPES, [-] Phenol red, 10% FBS)[Gibco, Denmark]). Compounds are shown in **Figure 1A**. Final compounds had >95% purity determined by high performance liquid chromatography (HPLC), high resolution mass spectrometry and NMR spectrometry. Liquid chromatography-mass spectrometry (LC-MS) and NMR spectrometry were used to determine the integrity and purity of all intermediates. THQ compounds were synthesized as described in schemes 1 and 2, which describe compounds MJM170 and JAG21 as exemplars. Building blocks 1, 8, 9 and 14 were varied to create the complete series (**Figure 1A**).

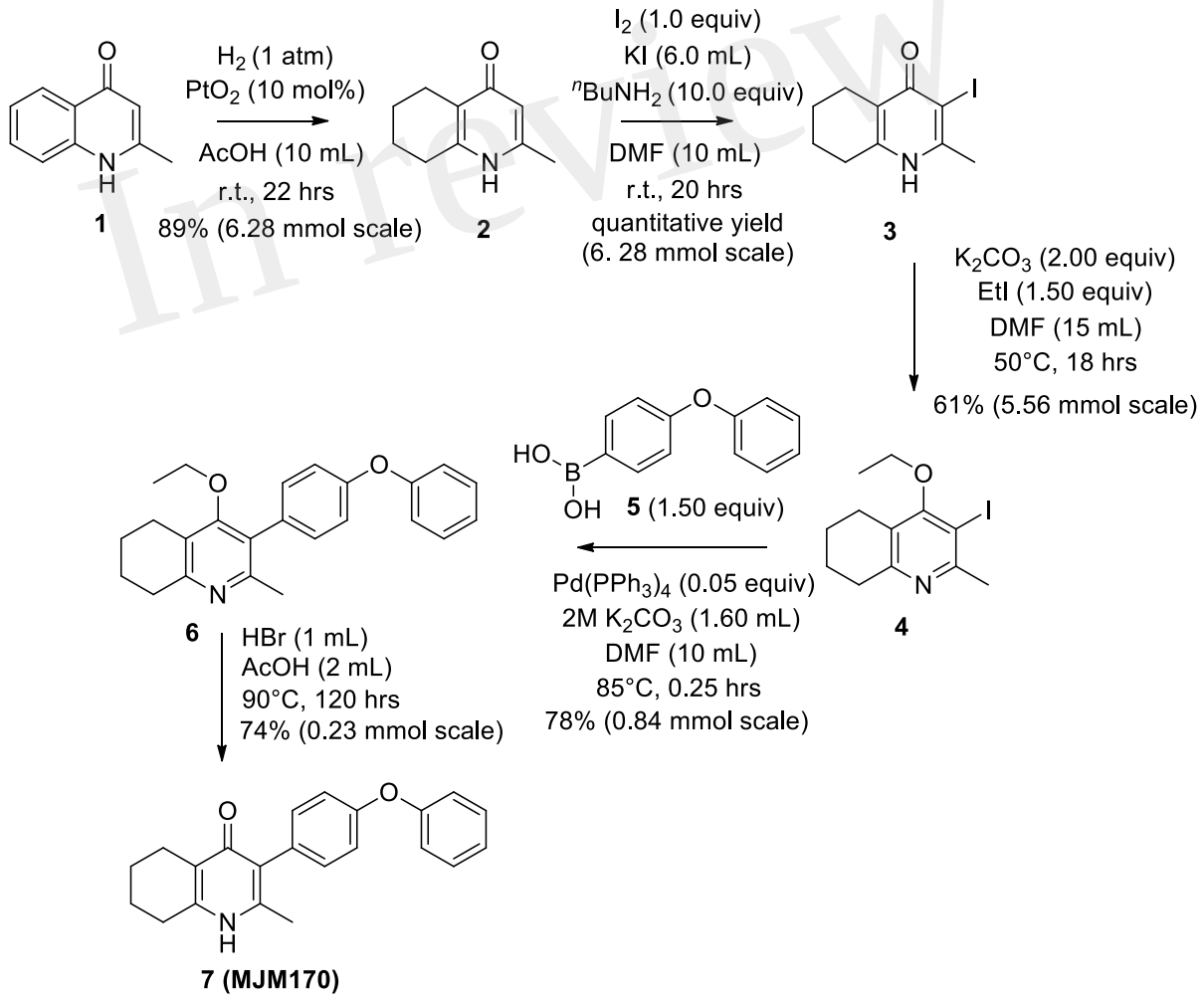

Scheme 1. Synthesis of hit compound 7, also known as MJM170 (McPhillie et al 2016**).** **Synthetic scheme inspired by the route to endochin-like quinolones (ELQs) reported by** Doggett et al, (2012**).**

Synthesis of 2-methyl-5,6,7,8-tetrahydroquinolin-4-one (2)

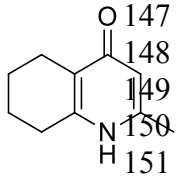

Platinum oxide (0.100 g, 10 mol %) was added to a solution of 4-hydroxy-2-methylquinoline (**1**, 1.00 g, 6.28 mmol, 1.00 eq) in glacial acetic acid (10.0 mL). The heterogeneous mixture was catalytically hydrogenated under a balloon of hydrogen. After 22 hrs, TLC (10% MeOH–DCM) confirmed complete reaction. The mixture was filtered through celite under vacuum, washing thoroughly with EtOAc (50 mL). The filtrate was concentrated and the resulting residue purified by column chromatography (10% MeOH–DCM) to give the desired product as a pale yellow oil (0.917 g, 5.65 mmol, 89%); $\boldsymbol{R_f}$ 0.14 (10% MeOH–DCM); **δ_H (300 MHz, $CDCl_3$)** 1.74-1.76 (4H, m, CH_2), 2.29 (3H, s, Me), 2.49-2.52 (2H, m, CH_2), 2.67-2.70 (2H, m, CH_2), 6.16 (1H, s, Ar-H); **δ_C (125 MHz, $CDCl_3$)** 19.0 (Me), 21.8 (CH_2), 22.1 (CH_2), 27.1 (CH_2), 112.5 (CH), 122.4 (Cq), 146.4 (Cq), 147.0 (Cq), 178.3 (Cq); Spectroscopic data consistent with literature values (JMC, 1993, 36, 1245-54).

Synthesis of 2-methyl-3-iodo-5,6,7,8-tetrahydroquinolin-4-one (3)

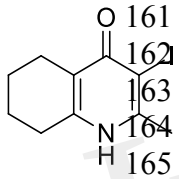

^{n}Butylamine (6.20 mL, 62.8 mmol, 10.0 eq) was added to a suspension of 2-methyl-5,6,7,8-tetrahydroquinolin-4-one (**2**, 1.02 g, 6.28 mmol, 1.00 eq) in DMF (10.0 mL). To this heterogeneous mixture was added I_2 (1.60 g, 6.28 mmol, 1.00 eq) in a saturated solution of KI (6.00 mL). After 20 hrs stirring at R.T., a precipitate formed in the orange solution, excess iodine was quenched with 0.1 M sodium thiosulfate solution (10.0 mL). The precipitate was filtered by vacuum filtration, washed with distilled H_2O and dried (Na_2SO_4) to give the desired product as a colourless solid (1.76 g, 6.09 mmol, quantative yield); **δ_H (300 MHz, DMSO-d_6)** 1.61-1.70 (4H, m, CH_2), 2.29 (2H, t, *J* 6.0, CH_2), 2.43 (2H, s, CH_2), CH_3 under DMSO peak.

Synthesis of 2-methyl-3-iodo-4-ethoxy-5,6,7,8-tetrahydroquinoline (4)

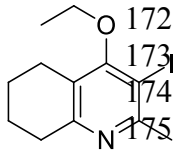

Potassium carbonate (1.53 g, 11.1 mmol, 2.00 eq) was added to a heterogeneous mixture of 2-methyl-3-iodo-5,6,7,8-tetrahydroquinolin-4-one (**3**, 1.60 g, 5.56 mmol, 1.00 eq) in DMF (15.0 mL), and the reaction heated to 50°C for 30 mins. The R.B. flask was removed from the heating mantle and ethyl iodide (0.67 mL, 8.33 mmol, 1.50 eq) was added dropwise. The reaction was then heated at 50°C for 18 hrs. The reaction was cooled to R.T., quenched with water (40 mL). The resulting emulsion formed which was extracted with EtOAc (50 mL). EtOAc layer were washed with water (3 x 30 mL), brine (3 x 30 mL), dried (Na_2SO_4) and concentrated to give a pale yellow oil (1.09 g, 3.44 mmol, 61%); $\boldsymbol{R_f}$ 0.88 (1:1 Pet–EtOAc); **HPLC** (RT = 1.67 mins); **LCMS** (Method A), (RT = 1.6 min, *m/z* (ES) Found MH^+ 318.0); **δ_H (500 MHz, $CDCl_3$)** 1.49 (3H, t, *J* 7.0, ethoxy CH_3), 1.73-1.78 (2H, m, CH_2) 1.84-1.88 (2H, m, CH_2), 2.78-2.69 (5H, m, CH_2 & CH_3), 2.84 (2H, t, *J* 6.5, CH_2), 3.97 (2H, q, *J* 7.0, OCH_2); **δ_C (125 MHz, $CDCl_3$)** 15.6 (CH_3), 22.3 (CH_2), 22.8 (CH_2), 23.6 (CH_2), 29.3 (CH_3), 32.0 (CH_2), 68.4 (OCH_2), 90.9 (Cq), 124.5 (Cq), 158.3 (Cq), 158.9 (Cq), 163.9 (Cq).

Synthesis of 2-methyl-3-(4-phenoxyphenyl)-4-ethoxy-5,6,7,8-tetrahydroquinoline (6)

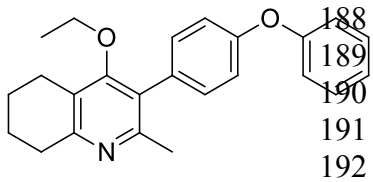

2-Methyl-3-iodo-4-ethoxy-5,6,7,8-tetrahydroquinoline (**4**, 0.266 g, 0.839 mmol, 1.00 eq), $Pd(PPh_3)_4$ (0.048 g, 0.0419 mmol, 5 mol%) and 4-phenoxyphenylboronic acid (**5**, 0.270 g, 1.26 mmol, 1.50 eq) were charged to a R.B. flask under N_2(g). Degassed DMF (10.0 mL) was added to the flask followed by 2M K_2CO_3 (1.60 mL). The flask was heated to 85°C under N_2(g). After 15 mins, TLC (4:1 Pet–EtOAc) confirmed reaction was complete. The reaction was cooled and diluted with EtOAc (15 mL), filtered through celite and partitioned between EtOAc (10 mL) and H_2O (25 mL). Combined organics were washed with H_2O (3 x 30 mL), then brine (3 x 30 mL), dried (Na_2SO_4) and concentrated to give a red oil which was purified by column chromatography (3:1 Pet–EtOAc), to give the desired product as a pale yellow oil (0.235 g, 0.655 mmol, 78%); ***R*$_f$** 0.31 (3:1 Pet–EtOAc); **HPLC** (RT = 3.08 mins); **δ_H (300 MHz, $CDCl_3$)** 1.04 (3H, t, *J* 7.0, ethoxy CH_3), 1.76-1.93 (4H, m, 2xCH_2), 2.32 (3H, s, CH_3) 2.72 (2H, t, *J* 6.0, CH_2), 2.91 (2H, t, *J* 6.5, CH_2), 3.50 (2H, q, *J* 7.0, OCH_2), 7.05-7.16 (5H, m, Ar-H), 7.20-7.29 (2H, m, Ar-H), 7.31-7.43 (2H, m, Ar-H); **δ_C (125 MHz, $CDCl_3$)** 15.7 (CH_3), 22.5 (CH_2), 23.0 (CH_3), 23.3 (CH_2), 23.4 (CH_2), 32.7 (CH_2), 68.2 (OCH_2), 118.6 (CH), 118.9 (CH), 123.4 (CH), 126.8 (Cq), 129.8 (CH), 131.5 (CH), 154.9 (Cq), 156.5 (Cq), 157.1 (Cq), 157.3 (Cq); ***m/z* (*ES*)** (Found: MH^+, 360.1973. $C_{24}H_{26}NO_2$ requires *MH*, 360.1964).

Synthesis of 2-methyl-3-(4-phenoxyphenyl)-4-ethoxy-5,6,7,8-tetrahydroquinoline (7, MJM170)

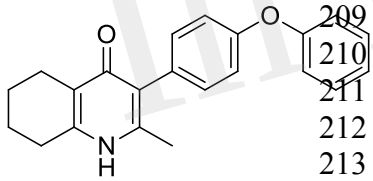

Aqueous hydrobromic acid (>48%) (1.00 mL) was added to a solution of 2-methyl-3-(4-phenoxyphenyl)-4-ethoxy-5,6,7,8-tetrahydroquinoline (**6**, 0.226 g, 0.630 mmol, 1.00 eq) in glacial acetic acid (2 mL). The reaction was stirred at 90°C for 5 days, monitoring by LMCS. The reaction was cooled to R.T. and the pH adjusted to pH 5 with 2M NaOH. The precipitate was collected by vacuum filtration and recrystallized from MeOH:H_2O to give the desired product as an off-white solid (0.155 g, 0.467 mmol, 74%); **HPLC** (RT = 2.56 mins); **δ_H (500 MHz, DMSO-*d*$_6$)** 1.66-1.72 (4H, m, 2xCH_2), 2.08 (3H, s, CH_3) 2.31 (2H, t, *J* 6.0, CH_2), 2.56 (2H, t, *J* 6.0, CH_2), 6.99 (2H, d, *J* 8.5, Ar-H), 7.06 (2H, d, *J* 7.5, Ar-H), 7.14-7.18 (3H, m, Ar-H), 7.40-7.43 (2H, m, Ar-H), 11.0 (1H, s, NH); **δ_C (125 MHz, DMSO-*d*$_6$)** 17.7 (CH_3), 21.5 (CH_2), 21.8 (CH_2), 21.9 (CH_2), 26.2 (CH_2), 117.8 (CH), 118.6 (CH), 121.2 (Cq), 123.3 (CH), 123.7 (Cq), 130.0 (CH), 131.4 (Cq), 132.3 (CH), 142.3 (Cq), 143.2 (Cq), 155.0 (Cq), 156.8 (Cq), 175.4 (Cq); ***m/z* (*ES*)** (Found: MH^+, 332.1654. $C_{22}H_{22}NO_2$ requires *MH*, 332.1645).

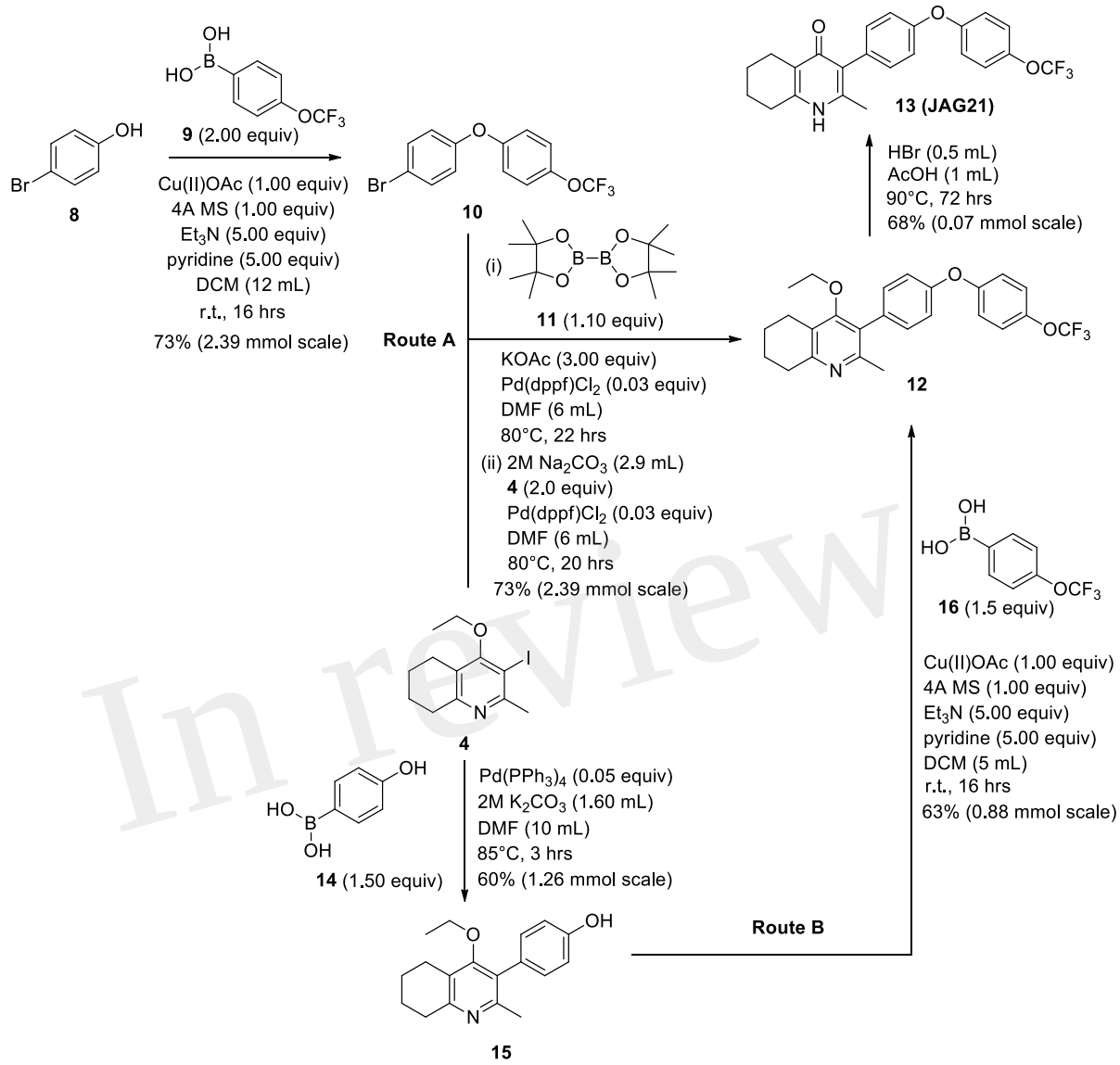

Scheme 2. Synthetic route to analogues of 7 (MJM170) via route A or route B. Route A is the original route to analogues but is linear and involves a tricky Suzuki step to intermediate 12 from intermediates 4 and 10. Route B allows quicker access to analogues since intermediate 15 can be made in larger quantities and derivatives can be synthesised via the Chan-Lam reaction to give final intermediate 12 by varying the boronic acid 16.

Synthesis of 1-(4-bromophenyl)-4-(trifluoromethoxy)benzene (10)

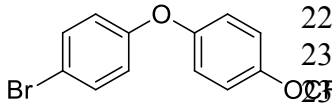

Copper (II) acetate (0.435 g, 2.39 mmol, 1.00 eq) was added to a suspension of 4-bromophenol (**8**, 0.414 g, 2.39 mmol, 1.00 eq), 4-trifluoromethoxybenzeneboronic acid (**9**, 0.983 g, 4.79 mmol, 2.00 eq) and 4Å molecular sieves (0.566 g) in DCM (12 mL) at R.T. A solution of triethylamine (1.7 mL, 11.9 mmol, 5.00 eq) and pyridine (1 mL, 11.9 mmol, 5.00 eq) was added and the reaction was stirred for 16 hrs, open to the atmosphere. After 18 hrs, the reaction was quenched with 0.5 M HCl (20 mL) and the organic layer washed with water (20 mL), brine (20 mL), dried (Na_2SO_4) and concentrated to give a red oil which was purified by

column chromatography (hexane) to give the desired product as a colourless oil (0.582 g, 1.75 mmol, 73%); ***R*f** 0.58 (hexane).

Synthesis of 2-methyl-3-(4-hydroxyphenyl)-4-ethoxy-5,6,7,8-tetrahydroquinolin-4-one (15)

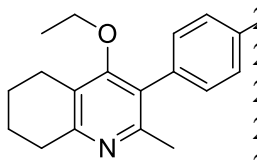

2-Methyl-3-iodo-4-ethoxy-5,6,7,8-tetrahydroquinoline (**4**, 0.400 g, 1.26 mmol, 1.00 eq), $Pd(PPh_3)_4$ (0.073 g, 0.06 mmol, 5 mol%) and 4-hydroxylphenylboronic acid (**14**, 0.260 g, 1.89 mmol, 1.50 eq) were charged to a R.B. flask under N_2(g). Degassed DMF (10.0 mL) was added to the flask followed by 2M K_2CO_3 (3.00 mL). The flask was heated to 85°C under N_2(g). After 3 hrs, TLC (EtOAc) confirmed reaction was complete. The reaction was cooled to 50°C, diluted with EtOAc (15 mL) and activated charcoal was added. After stirring for 30 mins, the mixture was filtered through celite and partitioned between EtOAc (10 mL) and H_2O (25 mL). Combined organics were washed with H_2O (3 x 30 mL), then brine (3 x 30 mL), dried (Na_2SO_4) and concentrated to give a brown solid which was triturated with diethyl ether to give the desired product as a pale red crystalline solid (0.220 g, 0.777 mmol, 60%); ***R*f** 0.22 (EtOAc); **m.p.** 225-226 °C (EtOAc); **δ_H (500 MHz, MeOD-*d*4)** 7.07 (d, *J* = 8.6 Hz, 2H, H-3 & 5), 6.86 (d, *J* = 8.6 Hz, 2H, H-2 & 6), 3.51 (q, *J* = 7.0 Hz, 2H, $CH_3\underline{CH_2}O$), 2.83 (t, *J* = 6.3 Hz, 2H, H-8'), 2.72 (t, *J* = 6.1 Hz, 2H, H-5'), 2.23 (s, 3H, Me), 1.95 – 1.72 (m, 4H, H-6' & 7'), 1.00 (t, *J* = 7.0 Hz, 3H, $\underline{CH_3}CH_2O$); **δ_C (125 MHz, MeOD-*d*4)** 164.0 (Cq), 158.1 (C-1), 157.4 (C_q), 156.1 (C_q), 132.2 (C-3 & 5), 129.1 (Cq), 127.9 (Cq), 124.9 (Cq), 116.2 (CH), 69.1 (OCH_2), 32.7 (CH_2), 23.9 (CH_2), 23.4 (CH_3), 22.9 (CH_2), 22.3 (CH_2), 15.7 (CH_3); ***m/z* (*ES*)** (Found MH^+, 284.1664, $C_{18}H_{21}NO_2$ requires *MH*, 284.1651).

Synthesis of 2-methyl-3-(4-hydroxyphenyl)-4-ethoxy-5,6,7,8-tetrahydroquinolin-4-one (12)

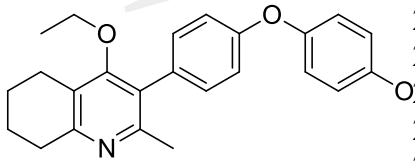

1-(4-bromophenyl)-4-(trifluoromethoxy)benzene (**10**, 0.100 g, 0.30 mmol, 1.00 eq), bis(pinacolato) diboron (1.10 eq), potassium acetate (3.00 eq) and $Pd(dppf)Cl_2$ (0.03 eq) were added to a oven-dried flask under inert (N_2) atmosphere. Anhydrous DMF (6 mL) was added and the reaction heated to 80°C under N_2 (g). After 22 hrs, the reaction was cooled to R.T., fresh $Pd(dppf)Cl_2$ (0.03 eq) added, followed by 2-methyl-3-iodo-4-ethoxy-5,6,7,8-tetrahydroquinoline (**4**, 0.400 g, 1.26 mmol, 2.00 eq) and 2M Na_2CO_3 (2.9 mL). The reaction was heated to 80°C for 20 hrs, cooled, diluted with EtOAc (20 mL), filtered through celite and partitioned between EtOAc (20 mL) and H_2O (20 mL). Combined organics were washed with brine (3 x 20 mL), dried (Na_2SO_4) and concentrated to give a brown solid which was purified by column chromatography (3:1 Pet–EtOAc) to give the desired product as a colourless oil (30 mg, 0.07 mmol, 23%); **HPLC** (RT = 2.41 mins); **δ_H (500 MHz, acetone)** 7.28 (d, *J* = 8.7 Hz, 2H, H-2' & 6'), 7.26 (d, *J* = 9.1 Hz, 2H, H-2'' & 6''), 7.09 (d, *J* = 9.1 Hz, 2H, H-3'' & 5''), 7.07 (d, *J* = 8.7, 2H, H-3' & 5'), 3.52 (q, *J* = 7.0 Hz, 2H, $CH_3\underline{CH_2}O$), 2.85 (t, *J* = 6.5 Hz, 2H, H-8), 2.78 (t, *J* = 6.2 Hz, 2H, H-5), 2.26 (s, 3H, Me), 1.89 – 1.81(m, 2H, H-7), 1.81– 1.72 (m, 2H, H-6), 0.93 (t, *J* = 7.0 Hz, 3H, $\underline{CH_3}CH_2O$); **δ_C (125 MHz, acetone)** δ 161.9 (Cq), 157.1 (Cq), 156.5 (Cq), 156.0 (Cq), 154.5 (Cq), 145.3 (Cq), 132.5 (Cq), 132.0 (CH), 126.7 (Cq), 123.0 (CH), 119.8 (CH), 119.0 (CH), 68.0 (OCH_2), 32.5 (CH_2), 23.0 (CH_2), 22.9 (CH_3), 22.7 (CH_2), 22.5 (CH_2), 15.05 (CH_3); ***m/z* (*ES*)** (Found: MH^+, 444.1792. $C_{25}H_{24}F_3NO_3$ requires *MH*, 444.1781).

Synthesis of 2-methyl-3-(4-(4-(trifluoromethoxy)phenoxy)phenyl)-5,6,7,8-tetrahydroquinolin-4-one (13, JAG21)

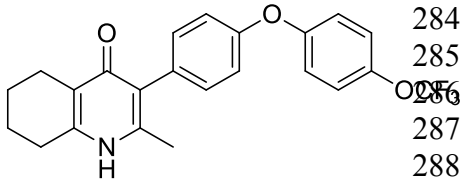

Aqueous hydrobromic acid (>48%) (1.00 mL) was added to a solution of 2-methyl-3-(4-phenoxyphenyl)-4-ethoxy-5,6,7,8- tetrahydroquinoline (**12**, 30.0 mg, 0.07 mmol, 1.00 eq) in glacial acetic acid (2 mL). The reaction was stirred at 90°C for 3 days, monitoring by LMCS. The reaction was cooled to R.T. and the pH adjusted to pH 5 with 2M NaOH. The precipitate was collected by vacuum filtration and recrystallized from MeOH:H_2O to give the desired product as a colourless solid (25.0 mg, 0.06 mmol, 68%); **m.p.** >250 ℃; **HPLC** (RT = 2.78 mins); **δ_H (500 MHz, DMSO-*d*$_6$)** 11.07 (s, 1H, NH), 7.40 (d, J = 8.5 Hz, 2H, H-2' & 6'), 7.19 (d, J = 8.6 Hz, 2H, H-3'' & 5''), 7.13 (d, J = 9.0 Hz, 2H, H-3' & 5'), 7.02 (d, J = 8.5 Hz, 2H, H-2'' & 6''), 2.54 (t, J = 6.0 Hz, 2H, H-8), 2.28 (t, J = 5.9 Hz, 2H, H-5), 2.07 (s, 3H, Me), 1.71 (m, 2H, H-7), 1.65 (m, 2H, H-6); **δ_C (125 MHz, DMSO-*d*$_6$)** 175.7 (Cq), 155.9 (Cq), 154.5 (Cq), 143.5 (Cq), 143.2 (Cq), 142.2 (Cq), 132.5 (CH), 132.2 (Cq), 123.6 (Cq), 123.0 (CH), 121.3 (Cq), 119.6 (CH), 118.2 (CH), 26.2 (CH_2), 21.9 (CH_2) 21.8 (CH_2), 21.5 (CH_2), 17.7 (CH_3); ***m/z* (*ES*)** (Found: MH^+, 416.1492. $C_{23}H_{20}F_3NO_3$ requires *MH*, 416.1473).

Toxoplasma gondii

Parasite Strains (Isolates)

RH-YFP tachyzoites, (McPhillie et al, 2016; Fomovska et al, 2012; Gubbels et al, 2003), EGS strain (Vidigal et al 2015; Paredes-Santos et al 2012;McPhillie et al, 2016), Pru-luciferase, Me49, and RPS13Δ on the RH strain background (Hutson et al, 2010) were prepared and passaged in human foreskin fibroblasts [HFF] as described.

T.gondii in vitro

In Vitro* Challenge Assay for *T.gondii

RH strain YFP Tachyzoites

Protocol was adapted from Fomovska, et. al (2012; 2012a) for HFF. HFF were cultured on a flat, clear-bottomed, black 96-well plate to 90%-100% confluence. IMDM (1x, [+] glutamine, [+] 25 mM HEPES, [+] Phenol red, 10% FBS [Gibco, Denmark]) was removed and replaced with IMDM-C(1x, [+] glutamine, [+] 25 mM HEPES, [-] Phenol red, 10% FBS)[Gibco, Denmark]). RH-YFP, lysed from host cells by passing twice through a 27-gauge needle, were counted, then diluted to 32,000/mL in IMDM-C. HFF were infected with 3200 RH-YFP, then returned to 37° C, CO_2 (5%) incubator for 1-2 hours for infection. Various concentrations of the compounds in 20 µl IMDM-C were added to each well. There were triplicates for each condition. Controls were pyrimethamine/sulfadiazine (standard treatment), 0.1% DMSO only, HFF only, and untreated cultures of HFF infected with 2 fold dilutions of YFP expressing parasites (called "YFP gradient" to establish amount of color from known numbers of YFP expressing parasites). Cells were incubated at 37° C for 72 hours. Plates were read using a fluorimeter (Synergy H4 Hybrid Reader, BioTek) to ascertain amount of relative fluorescence units (RFU) YFP, to measure parasite burden after treatment. Data were collected using Gen5 software with IC_{50} calculated by graphical analysis in Excel.

An initial screening assay of 10 µM, 1µM, 100 nM, and 10 nM of the compounds was performed. Compounds were not considered effective or pursued for further analysis if there was no inhibition of tachyzoites at 1µM. If compounds were effective at 1 µM, another experiment was performed to assess effect at 1 µM, 500 nM, 250 nM, 125 nM, 62.5 nM, and 31.25 nM.

Cytotoxicity Assays in parallel with RH Strain *T.gondii in vitro* studies

Toxicity assays used WST-1 cell proliferation reagent (Roche) as in Fomovska, et. al.(2012). HFF were grown on a flat, clear-bottomed, black 96-well plate. Confluent HFF were treated with inhibitory compounds at concentrations of 10 µM and 50 µM. Compounds were diluted in IMDM-C, and 20 µl were added to each designated well, with triplicates for each condition. A gradient with 2 fold-decreasing concentrations of DMSO from 10% to 0% in colorless, translucent IMDM-C was used as a control. The plate was incubated for 72 hours at 37° C. 10 µl WST-1 reagent (Roche) were added to each well. Cells were incubated for 30-60 minutes. Absorbance was read using a fluorimeter at 420 nm. A higher degree of color change (and absorbance) indicated mitochondrial activity and cell viability.

***In vitro* Challenge Assay for EGS strain Bradyzoites**

HFF cells were grown in IMDM on removable, sterile glass cover slips in the bottom of a clear, flat-bottomed 24-well plate. Cultures were infected with $3x10^4$ EGS strain parasites per well, in 0.5 mL media. The plate was returned to incubator at 37° C overnight. The following day, the media was removed. Colorless IMDM and compounds were added to make various concentrations of the drug. Total volume was 0.5 mL 2 wells had media only, as a control. Plates were returned to the 37° C incubator for 72 hours, checked once each 24 hours. If tachyzoites were visible in the control before 72 hours, cells were fixed and stained.

Cells were fixed using 4% paraformaldehyde and stained with Fluorescein-labeled Dolichos Biflorus Agglutinin, DAPI, and BAG1. Disks were removed, mounted on glass slides, and visualized using microscopy (Nikon Tl7). Slides were scanned using a CRi Panoramic Scan Whole Slide Scanner and viewed using Panoramic Viewer Software. Effects of compounds were quantitated by counting cysts in controls and treated cultures. Dolichos staining delimited structures and single organisms that remained were counted in a representative field of view. This was then multiplied by a factor determined by the total area of the cover slip in order to estimate the number of cysts and organisms in each condition. When the following forms were observed: "true cysts" with a dolichos-staining wall, "pseudocysts" or tight clusters of parasites, and small organisms, if there were fewer than four parasites visible in a cluster, organisms were counted individually (as "small organisms"). The entire scanned coveslip with all fields was also reviewed by 3 observers to confirm consistency.

Synergy studies with RH strain YFP Tachyzoites.

Atovaquone and pyrimethamine were used to test whether they are synergistic with JAG21. Serial dilutions of the combination of JAG21 and either atovaquone or pyrimethamine were used in an *in vitro* challenge assay as described above. The EC50 of each compound and the combination of two compounds were determined. The effect of the combination of drugs was calculated with the following formula:C= [A]c/[A]a+[B]c/[B]a. If C is lower than 1, the two compounds tested have

373 synergistic effect; if C is greater than 1, the two compounds tested have antagonist effect and if C
374 is 1 they are additive.
375
376 ***T.gondii* and HFF Mitochondrial Membrane Potential Measurements**—The mitochondrial
377 membrane potential was measured by the safranine method according to Vercesi et al, 1998).
378 Freshly egressed *T. gondii* tachyzoites were filtered and washed twice with intracellular buffer
379 (125 mM sucrose, 65 mM KCl, 10 mM HEPES-KOH buffer, pH 7.2, 1 mM $MgCl_2$ and 2.5 mM
380 potassium phosphate). After washing, the parasites were resuspended in the same buffer at 10^9/ml.
381 An aliquot of 50 µl of this suspension was added to a cuvette containing Safranin O, 2.5 µM and
382 Succinate 1 mM in final volume of 2 mL of the intracellular buffer. The fluorescence was measured
383 with a Hitachi 7000 spectrofluorometer with setting Ex. 495/Em. 586. Once the baseline
384 fluorescence is testable, 30 µM digitonin was added to permeabilize the parasites. 85 seconds after
385 permeabilization, the THQ derivatives, dissolved in DMSO, were added. 5 µM of FCCP (Carbonyl
386 cyanide-4-(trifluoromethoxy) phenylhydrazone) was used as an uncoupler reference for
387 calculations and its effect was considered 100%. We used similar conditions for measuring the
388 mitochondrial potential of mammalian cells with the following changes: The mammalian cells
389 were resuspended at 10^8/ml. We also used 50 µl of mammalian cells for each run in a cuvette with
390 2 µl solutions. The substrate used for mammalian cells was 5 mM glutamate and 5 mM malate. A
391 higher concentration of digitonin (50 µM) was used to permeabilize the mammalian cells. The
392 compounds were added at ~400 seconds after permeabilization. Each experiment was repeated at
393 least three times in duplicates. Statistical analysis, unpaired student t test, was performed using
394 GraphPad Prism 8.0 (GraphPad Software, Inc., San Diego, CA).

395 **Structure Activity Relationship (SAR) and comparison of effect on *T.gondii* and HFF enzyme**
396 **activity**.The effects of changing R1 as 7-Et, 7-Me, 6-CF_3, or 6-Me on activity against RH strain
397 tachyzoites. kinetic solubility, and metabolic stability were compared. Kinetic solubility and
398 metabolic stability in human or murine liver microsomes were measured. The hERG (human
399 Ether-à-go-go-Related) liability was also determined. The hERG gene (KCNH2) encodes a protein
400 K_v11.1, the alpha subunit of a potassium ion channel. This channel conducts the rapid component
401 of the delayed rectifier potassium current, IKr, which is critical for repolarization of cardiac action
402 potentials. A reduction in hERG currents from adverse drug effects can lead to long QT interval
403 syndromes. These syndromes are characterized by action potential prolongation, lengthening of
404 the QT interval on surface EKG, and an increased risk for "torsade de pointes" arrhythmias and
405 sudden death. The MDCK-MDR1 Permeability Assay was also performed. MDCK-MDR1 refers
406 to the ability of a compound to permeate across membranes of MDCK-MDR1 (Madin Darby
407 canine kidney [MDCK] cells with the *MDR1* gene [ABCB1], the gene encoding for the efflux
408 protein, P-glycoprotein (*P-gp)*) *in vitro*. Assessing transport in both directions (apical to
409 basolateral and basolateral to apical across the cell monolayers enables an efflux ratio to be
410 determined. This provides an indication as to whether a compound undergoes active efflux
411 (mediated by P-*gp*). This provides a prediction of blood brain barrier (BBB) penetration
412 potential/permeability and efflux ratio. Effect in CACO-2 (Colon Adenocarcinoma cells) as a
413 permeability assay and on cytochrome P450 CYP 450 were also determined. CYP enzymes
414 catalyze oxidative biotransformation (phase 1 metabolism) of most drugs. CYP enzymes,
415 bind to membranes in a cell (cyto) and contain a heme pigment (chrome and P) that absorbs
416 light at a wavelength of 450 nm when exposed to carbon monoxide. Metabolism of a drug by

417 CYP enzymes is a major source of variability in drug effect. These were measured by Chem
418 Partners. The relative effect on HFF and parasite enzymes also were compared. .

419

420 **RPS13Δ Tachyzoites in Human Primary Brain Neuronal Stem Cells *in vitro* for**
421 **transcriptomics and transcriptomics analyses**
422 Culture of Human Primary Brain Neuronal Stem Cells (NSC) was as described (McPhillie et al,
423 2016; Ngo et al, 2017); *T.gondii* RPS13Δ on RH strain background (Hutson et al, 2010) was used
424 to infect the NSC as described (McPhillie et al, 2016; Ngo et al, 2017). RNA was isolated and
425 prepared and used for transcriptomic experiments as dervribed (McPhillie et al, 2016; Ngo et al,
426 2017).Briefly, NSC, initially isolated from a temporal lobe biopsy (Walton et a, 2006) were
427 infected with either wild-type or RPS13Δ RH tachyzoites using biological duplicates at a
428 multiplicity of infection of 2:1 and incubated as previously described (Ngo et al, 2017). Eighteen
429 hours post-infection, extracellular parasites were washed out with cold PBS before total RNA
430 extraction. Further isolation of the mRNA fraction was carried out with miRNeasy Mini Kit
431 columns (Qiagen) following manufacturer instructions and Illumina barcoded mRNA sequencing
432 libraries were constructed with TruSeq RNA Sample Preparation Kits v2 (Illumina). Libraries
433 were sequenced as 100 bp single reads with Illumina HiSeq 2000 apparatus at a sequencing depth
434 of ~3 Gbp per sample. Sequencing reads were mapped to the human (release GRCh38) and *T.*
435 *gondii* ME49 strain (ToxoDB release 13.0) reference genome assemblies with hisat2 (Kim et
436 al,2015) and raw read counts were per gene were estimated with HTSeq (Anders et al,
437 2015). Identification of parasite genes that were differentially expressed between wild-type
438 and RPS13Δ parasites was performed with the R package DESeq2 (Love et al, 2014) using a
439 generalized linear model likelihood ratio test. Identification of orthologous genes between *T.*
440 *gondii* and *P. cynomolgi* was carried out by best-reciprocal matches between *T. gondii* and *P.*
441 *cynomolgi* proteomes using Blastp and a e-value cutoff of 1 x 10^{-3}. The list of Genes that are
442 differentially expressed between *P. cynomolgi* hypnozoites and the liver-schizont stage was
443 extracted from a previously published study by Cubi R. et al (Cubi et al, 2017l). Gene set
444 enrichment analysis was carried out with the GSEA tool (Subramanian et al, 2005) using *T.*
445 *gondii* Gene Ontology and cell cycle gene sets developed by Croken M et al (Croken et al, 2014l)
446 and visualized with the Enrichment Map application in Cytoscape (Su et al,2014).
447
448

449 ***T.gondii in vivo***

450 **Type II parasites *in vivo***

451 **IVIS.** Balb/C mice were infected intraperitoneally (IP) with 20x10^3 *T. gondii* (Prugneaud strain
452 expressing luciferase) tachyzoites. Treatment began 2 hours later with JAG21 (5mg/kg) which was
453 dissolved in DMSO, administered IP in a total volume of 0.05ml. Mice were imaged every second
454 day starting on day 4 post infection using an IVIS Spectrum (Caliper Life Sciences) for minute
455 exposures, with medium binning, 20 minutes post injection with 150 mg/kg of D-luciferin
456 potassium salt solution.

457 **Brain cysts**:

458 Brain cysts were searched for in paraffin imbedded tissue of the surviving Prugneaud strain
459 infected treated Balb/C mice in the IVIS study, 30 days after infection which was 16 days after
460 treatment had been discontinued. All treated mice had survived. There were no surviving untreated
461 mice in those experiments.
462
463 In separate experiments, Balb/C mice were infected IP with 20 x 10^3 *T. gondii* Me49 strain
464 tachyzoites. In these separate studies of mice with established chronic infection, after 30 days, IP
465 treatment with JAG21 was begun each day for 14 days. JAG21 was dissolved in DMSO and
466 administered IP in a total volume of 0.05ml. In experiments when tafenoquine was administered
467 alone or with JAG21 in some groups 3mg/kg tafenoquine was administered once on day -1 from
468 when JAG21 treatment was initiated. Cysts in brain were quantitated on day 30, 16 days after
469 discontinuing JAG21. Immunoperoxidase staining was performed. Parasite burden was
470 quantitated in two ways. The first was using a positive pixel count algorithm of Aperio ImageScope
471 software. Positive pixels were normalized to tissue area (mm^2). Briefly, automated quantitation
472 was done by counting positive pixels per square area. The entire brain in one section was scanned
473 for each mouse. The Cyst burden was quantitated as units of positive pixels per
474 mm2. The average +/- S.E.M. numbers of mm2 per slide quantitated was 30.2+/-1.6 square mm
475 per mouse for this quantification. Each highpower field of view shown in **Fig.5C** is
476 approximately 0.02 mm^2 per field of view. Cysts on each slide for each condition in two
477 biological replicate experiments were also quantitated by 2 separate observers independently and
478 results compared with automated counting, separately.
479
480 **RPS13 Δ *in vivo***
481
482 This G1 arrested parasite persists in tissue culture for prolonged times in the absence of tetracycline
483 (Hutson et al 2010), but in immune competent mice it cannot be rescued with teteracycline, or
484 LNAME (L-N^G-Nitro arginine methyl ester, an analog of arginine) used as an antagonist of nitric
485 oxide synthase (NOS) that inhibits NO production, or both together (Hutson et al 2010).
486
487 In pilot studies, herein, interferon γ receptor knockout mice that were not treated were observed
488 following infection. At 7 and at 14 days following infection, spleen and liver were removed and
489 immune peroxidase stained. At 14 days a group of mice were treated with anhydrotetracycline and
490 when a subset of these mice died their spleen and liver were removed and immune peroxidase
491 stained.

492 As in the pilot studies, this RPS13 Δ parasite also was used to infect interferon γ receptor knockout
493 mice in a treatment study. The design of this experiment with these immune compromised mice is
494 shown in **Fig. 6**. In this separate study, groups of mice were infected with RPS13 Δ. They were
495 treated with tafenoquine on day -1, or JAG21 for 14 days 2 hours after infection, or the two together
496 with tafenoquine on day -1 and JAG21 for the first 14 days, or with diluent only for 14 days, as
497 described above. For the initial 14 days no tetracycline was administered. After that time
498 tetracycline was administered. Mice were observed each day. At the time they appeared to have
499 substantial illness or at the termination of the experiment they were euthanized, tissues fixed in
500 formalin and stained with hematoxylin and eosin or immunoperoxidase stained and parasite burden
501 was assessed.

502 **RH challenge in a study of oral administration of a novel nano formulation of JAG21**.:

503 **Nanoformulation of JAG21 for oral administration in *T.gondii* studies**. JAG21 was prepared
504 using hydroxyethyl cellulose (HEC) and Tween 80. Briefly, this dispersant solution containing
505 5mg/mL HEC and 2mg/mL Tween 80 in water was prepared. Solid JAG21 was added to
506 20mg/mL, and the dispersion was sonicated for 60 seconds using a Sonics vc50 probe-tip sonicator
507 set to 20kHz to homogenize. Sonication was performed at room temperature. Aliquots of the
508 homogeneous dispersion were frozen and lyophilized using a VirTis AdVantage freeze drier.
509 These aliquots were stored at room temperature for 5-6 months. Prior to dosing, aliquots were
510 reconstituted using water. Controls containing no JAG21 were also prepared. Following
511 reconstitution with water, the dispersion was imaged using a Nikon ECLIPSE E200 optical
512 microscope set to 40x magnification. The average particle size of the JAG21 dispersion in
513 HEC/Tween 80 was determined using an in-house image analysis program This novel method to
514 stably formulate JAG21 was discovered after all other studies were completed and this was the last
515 experiment in this manuscript performed as a consequence.

516 **RH YFP challenge**. For studies of the nano formulated JAG 21, this was administered for one or
517 three days by gavage in the doses shown in the results section. These C57BL6 background mice
518 received 2000 RH tachyzoites IP. on day the first day of the experiment and peritoneal fluid was
519 collected 5 days later to quantitate flluorescence and numbers of parasites.

520 **Malaria assays**
521
522 **Enzyme assays:**
523
524 Methods for enzyme assays:
525 Materials
526 *P. falciparum* 3D7 strain were obtained from the Liverpool School of Tropical Medicine. Protease
527 cocktail inhibitor was obtained from Roche. Bradford protein assay dye reagent was obtained from
528 Bio-Rad. All other reagents were obtained from Sigma-Aldrich. Decylubiquinol was produced as
529 per Fisher et al.(2009). In brief, 25 mg of decylubiquinone were dissolved in 400 µl of nitrogen-
530 saturated hexane. An equal volume of aqueous 1 M sodium dithionite was added, and the mixture
531 vortexed until colorless. The organic phase containing the decylubiquinol was collected, the
532 solvent was evaporated under N_2 and the decylubiquinol finally dissolved in 100 µl of 96% ethanol
533 (acidified with 10 mM HCl). Concentrations of decylubiquinol was determined
534 spectrophotometrically on a Cary 300 Bio UV/visible spectrophotometer (Varian, UK) from
535 absolute spectra, using $\varepsilon_{288-320}$ = 8.1 mM-1 .cm^{-1}. Decylubiquinol was stored at -80 °C and used
536 within two weeks.
537
538 *P. falciparum* culture and extract preparation
539 *P. falciparum* strain 3D7 blood-stage cultures were maintained by the method of Trager and Jensen
540 (1976). Cultures contained a 2% suspension of O+ human erythrocytes in RPMI 1640 medium
541 containing L-glutamine and sodium carbonate, and supplemented with 10% pooled human AB+
542 serum, 25 mM HEPES (pH 7.4) and 20 µM gentamicin sulphate. Cultures were grown under a
543 gaseous headspace of 4 % O_2 and 3% CO_2 in N_2 at 37°C. Cultures were grown to a parasitemia of
544 5 % before use.

545
546 The protocol for the preparation of parasite extract was adapted from Fisher et al.[30]. Free parasites
547 were prepared from infected erythrocytes pooled from five T75 flasks, by adding 5 volumes of
548 0.15% (w/v) saponin in phosphate-buffered saline (137 mM NaCl, 2.7 mM KCl, 1.76 mM
549 K_2HPO_4, 8.0 mM Na_2HPO_4, 5.5 mM D-glucose, pH 7.4) for 5 min, followed by three washes by
550 centrifugation in RPMI containing HEPES (25 mM), and a final resuspension in potassium
551 phosphate buffer (50 mM K_2HPO_4, 50 mM KH_2PO_4, 2 mM EDTA, pH7.4) containing a protease
552 inhibitor cocktail (Complete Mini; Roche). Parasite extract was then prepared by disruption with
553 a sonicating probe for 5 s, followed by a 1 min rest period on ice to prevent the sample overheating.
554 This process was performed three times. The parasite extract was used immediately. The protein
555 concentration of the parasite extract was determined by Bradford protein assay (Bio-Rad).
556
557 $Pfbc_1$ native assay
558 *P. falciparum* bc_1 complex cytochrome c reductase (*$Pfbc_1$*) activity was measured by monitoring
559 cytochrome c reduction at 550 versus 542 nm using a Cary 300 Bio UV-Visible Spectrophotometer
560 (Varian, UK), using a protocol adapted from Fisher et al. (2009).The assay was performed in
561 potassium phosphate buffer in a quartz cuvette and in a final volume of 700 µL. Potassium cyanide
562 (10 µM), oxidized cytochrome c (30 µM), parasite extract (100 µg protein) and compound/DMSO
563 were added sequentially to the cuvette, with mixing between each addition. Test compounds were
564 added to a final concentration of 1 µM. DMSO (0.1% v/v) and atovaquone (1 µM), a known
565 malarial cytochrome bc_1 complex inhibitor, were used as negative and positive controls
566 respectively. The reaction was initiated by the addition of 50 µM decylubiquinol and allowed to
567 proceed for 3 min.
568
569 **Malaria parasite *In vitro* studies:**
570 Malaria potency testing in vitro was performed using 4 different *P. falciparum* strains, D6, TM91-
571 C235, W2, and C2B. The D6 strain is a drug sensitive strain from Sierra Leone, the TM91-C235
572 strain is a multi-drug resistant strain from Thailand, the W2 strain is a chloroquine resistant strain
573 from Thailand, and the C2B strain is a multi-drug resistant strain with resistance against
574 atovaquone. These assays were performed as described below.
575
576 Compound Activity against *Plasmodium falciparum*
577 Compound activity against *P. falciparum*, was tested using the Malaria SYBR Green I - Based
578 Fluorescence (MSF) Assay. The complete method for performing this microtiter assay is described
579 in previous work published by Plouffe et al.(2008) and Johnson et al (2007). In brief, this assay
580 uses the binding of the fluorescent dye SYBR Green I to malaria DNA to measure parasite growth
581 in the presence of two-fold diluted experimental or control. The relative fluorescence of the
582 intercalated SYBR Green I proportional to parasite growth, and inhibitory compounds will result
583 in lower observed fluorescence compared to untreated parasites.
584
585 Cytotoxicity assays in parallel with *P.falcipaum* assay*s in vitro*
586 Toxicity studies also were performed with HepG2 cells (human liver cancer immortal cell line
587 derived from the liver tissue of a 15-year-old African American, ATCC ^{R} HB-8065^{TM}) in
588 parallel with the studies of *P.falciparum,* with inhibitors in vitro , as described in McPhillie et al
589 (2016).
590

591 ***P. berghei* causal prophylaxis *in vivo* model**
592 *P. berghei* sporozoites were obtained from laboratory-reared female *Anopheles stephensi*
593 mosquitoes which were maintained at 18 degrees C for 17-22 days after feeding on a luciferase
594 expressing *P. berghei* infected Swiss CD1ICR Using a dissecting microscope, the salivary glands
595 were extracted from malaria-infected mosquitoes and sporozoites were obtained. Briefly,
596 mosquitoes were separated into head/thorax and abdomen. Thoraxes and heads were triturated
597 with a mortar and pestle and suspended in medium RPMI 1640 containing 1% C57BL/6 mouse
598 serum (Rockland Co, Gilbertsville, PA, USA). 50–80 heads with salivary glands were placed into
599 a 0.5 ml Osaki tube on top of glass wool with enough dissection media to cover the heads. Until
600 all mosquitoes had been dissected, the Osaki tube was kept on ice. Sporozoites that were isolated
601 from the same batch of mosquitoes were inoculated into C57BL/6, 2D knock-out and 2D knock-
602 out/2D6 knock-in C57BL/6 mice on the same day to control for biological variability in sporozoite
603 preparations. On day 0, each mouse was inoculated intravenously in the tail vein with
604 approximately 10,000 sporozoites suspended in 0.1 ml volume. They were stained with a vital dye
605 containing fluorescein diacetate (50 mg/ml in acetone) and ethidium bromide (20 μg/ml in
606 phosphate buffered saline; Sigma Chemical Co, St. Louis, MO, USA) and counted in a
607 hemocytometer to ensure that inoculated sporozoites were viable following the isolation
608 procedure. Viability of the sporozoites ranged from 90 to 100%.
609
610 Animals
611 The mice used in these experiments were albino C57BL/6 female mice which were housed in
612 accordance with the current Guide for the Care and Use of Laboratory Animals (1996) under an
613 IACUC approved protocol. All animals were quarantined for 7 days upon arrival, and the animals
614 were fed standard rodent maintenance food throughout the study.
615
616 Test compounds, homogenization of JAG21 creating a nanoformulation, and administration
617 Animals were dosed with experimental compounds based on body weight. The suspension solution
618 of orally administered drugs were conducted in 0.5% (w/v) hydroxyethyl cellulose and 0.2%
619 Tween 80 in distilled water. To insure the size of the compounds in the dosing solution were under
620 50 μM (measured they were 4-6 μ), the suspension was homogenized using a homogenizer (PRO
621 Scientific Inc, Monroe, CT, USA) with a 10 mm open-slotted generator running at 20,000-22,000
622 rpm for 5 min in an ice bath. The compounds were made fresh each day and used immediately
623 (always in <1/2 hour). Stability beyond that time was not determined. It was not anticipated that
624 they would be stable beyond that time.
625
626 Compounds were administered on 3 consecutive days (−1, 0, +1) relative to sporozoite infection
627 or a single dose on day 0. Drug suspensions were administered to mice by oral gavage using an 18
628 gauge intragastric feeder. For the 3 day dosing regimen, compounds were administered at 0.625
629 mg/kg and for the single dose regimen administered on day 0, compounds were administered at
630 2.5 mg/kg.
631
632 *In vivo* imaging
633 All of the i*n vivo* bioluminescent imaging methods utilized have been described previously.
634 Briefly, JAG21 was administered orally on days −1, 0 and 1 with respect to sporozoite inoculation.
635 All inoculated mice were imaged using the Xenogen IVIS-200 Spectrum (Caliper Life Sciences,
636 Hopkinton, MA, USA) IVIS instrument at 24, 48 and 72 hours post-sporozoite infection. The

637 bioluminescent imaging experiments were conducted by IP injection of the luciferase substrate,
638 D-Luciferin potassium salt, (Xenogen, California and Goldbio, St Louis, MO, USA), into mice at
639 a concentration of 200 mg/kg 15 min before bioluminescent images were obtained. Three minutes
640 after luciferin administration the mice were anesthetized using isoflurane, and the mice were
641 positioned ventral side up on a 37degree C platform with continual anesthesia provided through
642 nose cone delivery of isoflurane. All bioluminescent images were obtained using 5minute
643 exposures with f-stop = 1 and large binning setting. Photon emission from specific regions was
644 quantified using Living Image® 3.0 software (Perkin Elmer),
645
646 Additionally, blood stage parasitemia was assessed 3 days after imaging was completed by treating
647 small quantities of blood obtained from tail bleeds with the fluorescent dye Yoyo-1 measured by
648 using a flow cytometry system (FC500 MPL, Beckman Coulter, Miami, FL, USA), (Pybus et al,
649 2013; Marcissin et al, 2014)
650
651
652 **Methods for Co-Crystallization and binding studies**

653 Bovine cytochrome bc_1 activity assays.

654 Bovine cytochrome bc_1 inhibition assay was carried out in 50mM KPi pH 7.5, 2 mM EDTA,
655 10mM KCN, 30μM equine heart cytochrome *c* (Sigma Aldrich), and 2.5 nM bovine cytochrome
656 bc_1 at room temperature. 20 mM inhibitors dissolved in DMSO were added to the assay at a desired
657 concentration without prior incubation. The working concentration of DMSO in the assay did not
658 exceed 0.3% v/v. The reaction was initiated by the addition of 50 μM decylubiquinol (Abcam).
659 The reduced cytochrome *c* was monitored by the different absorption between 550 and 542 nm
660 using extinction coefficient of 18.1 $mM^{-1}cm^{-1}$ in a SPECTRAmax Plus 384 UV-visible
661 Spectrometer. The initial kinetic rate is determined as a zero-order reaction and used as the specific
662 activity of cytochrome bc_1.

663 Bovine Cytochrome bc1 purification protocol:

664 Preparation of crude mitochondria

665 Whole fresh bovine heart was collected after slaughter and transported in ice. All work was carried
666 out at 4 °C. Lean heart muscle was cut into small cubes and homogenized in the buffer composed
667 from 250 mM sucrose; 20 mM K_2HPO_4; 2 mM succinic acid; 0.5 mM EDTA. Buffer was added
668 at a ratio of 2.5L per 1 kg of muscle tissue. Ph of resulting homogenate was adjusted to 7.8 using
669 2 M Tris and PMSF protease inhibitor was added to 0.1 mM concentration. The homogenate was
670 then centrifuged in a Sorvall GS-3 rotor at 5000g for 20 mins. The resulting supernatant was then
671 transferred to a Sorvall GSA rotor and centrifuged at 20,000g for 20 mins. Obtained mitochondrial
672 pellet was washed in 50 mM KPi (pH 7.5); 0.1 mM PMSF buffer before second centrifugation
673 under the same condition. The pellet was collected and sored at -80 °C for further use.

674 Solubilisation of membrane proteins

675 The frozen mitochondria were thawed and re-suspended in 50 mM KPi (pH 7.5); 250 mM NaCl;
676 0.5mM EDTA; 0.1 mM PMSF buffer; a small sample was taken for quantification of total
677 mitochondrial proteins by BCA assay. The remaining sample was centrifuged at 180,000g in

678 Beckman Ti70 rotor for 60 mins. The pellet was re-suspended in the same wash buffer with the
679 addition 1 mg DDM per 1 mg of protein and then centrifuged under the same conditions for 60
680 mins. The pellet was discarded and the supernatant was collected for ion exchange
681 chromatography.

682 Purification of cytochrome bc1

683 During purification the presence of protein was detected using 280 nm absorbance and the presence
684 of heme was detected using 415 nm Soret band peak and 562 nm absorbance. The solubilized
685 protein solution was applied on DEAE-Sepharose CL-6B column (ca. 50 ml, GE Healthcare) pre-
686 equilibrated with buffer A (50 mM KPi (pH 7.5); 250 mM NaCl; 0.01 % w/v DDM; 0.5mM
687 EDTA) and washed with 3 CV of buffer A. The protein was eluted by linear gradient with buffer
688 B (50 mM KPi (pH 7.5); 500 mM NaCl; 0.01%w/v DDM; 0.5mM EDTA). Fractions containing
689 cytochrome bc_1 were pooled and concentrated to 0.5 ml using an Amicon Ultra-15 (Amicon,
690 MWCO 100,000) concentrator. Concentrated sample was applied to a Sephacryl-S300 gel
691 filtration column (ca. 120 ml) pre-equilibrated in buffer C (20 mM KMOPS (pH 7.2); 100 mM
692 NaCl; 0.01%w/v DDM; 0.5 mM EDTA) and eluted at a flow rate of 0.5 ml/min. Purified
693 cytochrome bc_1 fractions were collected and concentrated to 40 mg/m. PEG fractionation with
694 increasing concentration of PEG4000 was used to precipitate cytochrome bc_1. Precipitating
695 solution (100 mM KMES pH 6.4; 10% PEG4000; 0.5 mM EDTA) was mixed with the protein to
696 a desired PEG concentration. The precipitated protein pellet was re-solubilised in buffer D (25
697 mM KPi pH 7.5, 100 mM NaCl, 0.5 mM EDTA, 0.015% DDM) and dialysed in the same buffer
698 in a centrifugal ultrafilter to remove residual PEG. 5 μM cytochrome bc_1 was incubated at 4 ºC for
699 12 hours with 50 μM JAC021 (10-fold molar excess) diluted from 20mM solution stock in DMSO.
700

701 Crystallization, data collection and refinement of Cytochrome bc1 - JAG021 complex
702

703 The inhibitor-bound cytochrome bc_1 was mixed with 1.6% HECAMEG to the final protein
704 concentration of 40 mg/mL. Hanging drop methods was used for crystallisation. 2 μL of final
705 protein solution with 2 μL of reservoir solution (50 mM KPi pH 6.8, 100 mM NaCl, 3 mM NaN_3,
706 10-12% PEG4000) was equilibrated over reservoir solution at 4 ºC. The crystals were grown to
707 100 μm within four days. The single crystal was transferred in reservoir solution containing
708 increasing to 50% concentrations of ethylene glycol prior to cryo-cooling in liquid nitrogen. X-ray
709 data were collected from single crystal PROXIMA2 beamline, SOLEIL light source, France using
710 DECTRIS EIGER X 9M detector at 0.9801Å wavelength up to 3.45Å resolution. Data were
711 indexed and integrated using iMosflm (Battye et al, 2011), and scaled using Aimless (Evans,
712 2011). The starting model for refinement was 5OKD. All ligands except co-factors were removed
713 from the model prior to refinement. Jelly-body refinement was carried out with Refmac5
714 (Murshudov et al, 2011). The inhibitor model was generated by Jligand (Lebedev et al, 2012). The
715 model was manually edited in COOT (between cycle refinements. Data collection and refinement
716 statistics are shown in Supplemental Table S1).
717
718

719 **Co-cryo electron microscopy**

720 **Electron microscopy and image processing**

721 Cryo-EM was carried out as described in Amporndanai et al. (2018). Briefly, 3 µL of sample at 5
722 mg/mL concentration were applied to Quantifoil Cu R1.2/1.3, 300 mesh holey carbon grids and
723 plunge frozen using an FEI Vitribot (blot time 6 seconds, blot force 6). Data were collected on an
724 FEI Titan Krios with a Falcon III direct electron detector operated in integrating mode at 300 kV.
725 Automated data collection was carried out using EPU software with a defocus range of -1 to -3.5
726 µm, and a magnification of 75,000 x which yielded a pixel size of 1.065 Å. Data were collected
727 for 72 hours resulting in 5,356 micrographs. The total dose was 66.4 e^-/Å over a 1.5 second
728 exposure which was split into 59 frames. All of the processing was performed in RELION 2.1
729 unless otherwise stated. The initial drift and CTF correction was carried out using
730 MOTIONCORR2 (Zheng et al, 2017) and Gctf (Zhang,et al., 2016) respectively. The micrographs
731 were examined and those with crystalline ice were initially removed resulting in 2,960
732 micrographs. A subset of ~2,000 particles were manually picked to generate 2D references to
733 facilitate auto-picking resulting in 439,009 particles. These particles underwent an initial round of
734 2D classification with those classes that displayed clear secondary structure detail being taken
735 forward to 3D classification and split into three classes. Two of the three classes generated a high-
736 quality cytochrome bc_1 reconstruction with secondary structure information clearly visible. The
737 particles from these two classes were recombined to form the final datasets consisting of 211,916
738 particles in the final reconstruction. The particles were 3D refined using C2 symmetry to produce
739 a map with resolution 3.8 Å. The particles also underwent movie refinement and particle polishing
740 which further improved the resolution of the map to 3.7 Å. A previously refined EM structure for
741 SCR0911 (pdb 6FO6) was fit into the map using UCSF chimera and subsequently refined using
742 phenix with the correct ligand. The maps were then inspected manually in COOT (Emsley et al
743 2004) and the model corrected for any errors in refinement and the placement of residues.
744
745 **Statistical Analysis**
746 A Pearson test was used to confirm a correlation between increasing dose and increasing inhibition.
747 An ANOVA and subsequent pairwise comparison with Dunnett correction was used to determine
748 whether or not inhibition or toxicity at a given concentration was statistically significant. Stata/SE
749 12.1 was used for this analysis.
750
751
752
753 **RESULTS**
754
755 **THQ compounds are potent *in vitro***

756 Initially, a small library of seven compounds **(Figs. 1 [**blue and green font, **Fig. 1A] and 2**) were
757 tested, and each compound was tested at least twice against *T. gondii* tachyzoites. JAG021 and
758 JAG050 demonstrated effect below 1 µM, and were tested at lower concentrations. JAG050 and
759 JAG021 were identified as lead compounds given the IC_{50} values obtained were 33 and 55 nM,
760 respectively. Correlation between concentration of compound and inhibition of parasite replication
761 (as measured by fluorescence) was observed for all compounds except JAG046. The relative effect
762 on HFF and parasite enzymes were also compared, with those marked ** in **Fig. 1A** having the
763 most effect on the parasite enzyme activity relative to host HFF enzyme activity as shown below
764 in **Fig 3**.

765 A representative graph of these *in vitro* data is shown in **Fig. 2A.** Subsequently, a larger library of
766 54 compounds was synthesized to ascertain structure-activity relationships (SAR) (**Fig. 1B**). Our
767 primary aims were to block putative metabolism of the terminal phenol ring of MJM170 and
768 improve the solubility across the compound series. Substituents were generally tolerated at the
769 meta and para positions on the phenol ring (R_1), similar to the trends observed in the ELQ series
770 (McPhillie et al, 2016; Dogget et al 2012, Vidigal et al 2002*)*. The incorporation of heteroatoms
771 into the aryl rings of the biphenyl moiety did not lead to improvements in solubility and biological
772 activity. Small substituents were tolerated at the 7-position of the THQ bicyclic ring (**Fig. 1B**; R_1**)**,
773 improving selectivity (see below, SAR) but not at the 6-position unlike the ELQ series. In
774 summary, overall, nitrogen atoms not tolerated in aryl ring (C) and the 4-position was optimal for
775 phenol substituent**.** Ultimately, no other compound had all the advantages of JAG21, although
776 some of these were identified as potential back up compounds(marked with **), with greater
777 selectivity for the parasite relative to the mammalian enzyme activity. Compound JAG21
778 displayed synergy against RH strain tachyzoites with atovaquone (**Fig. 2C**) but not with
779 pyrimethamine, although no antagonism was observed (data not shown).
780
781 Cytotoxicity assays performed in parallel using HFF, WST-1 (Fomovska et al, 2012; Fomovska,
782 et al 2012a) , and HEP G2 cells demonstrated a lack of toxicity at concentrations substantially in
783 excess of the concentrations effective against tachyzoites. Because *T. gondii* grows inside cells, if
784 a compound were toxic to host HFF then it would make the compound appear to be spuriously
785 effective (Fomovska et al, 2012; Fomovska, et al 2012a), when in actuality only toxicity for the
786 host cell would be measured. Cytotoxicity to HFF was therefore assessed for all compounds at 10
787 μM. Results of this experiment are in **Fig. 1A,** toxicity column. A two-way ANOVA and
788 subsequent pairwise comparison found none of the differences in absorbance, compared to the
789 media-DMSO vehicle controls, to be statistically significant ($p>0.05$). Most of these compounds
790 are not toxic at 10μM (the limit of solubility) and that cytotoxicity to cells can be attributed to
791 DMSO in the solution, not the compound. Dose response testing (IC50) was performed with HEP
792 G2 cells as described and the observed toxicity was: HEP G2 IC50 17.70 μM (r^2= 0.97) for
793 JAG021; 7.1 μM (r^2= .98) for JAG050.
794
795 Lead compounds JAG050, JAG021 and others were tested against EGS strain(McPhillie et al,
796 2016; Vidigal et al, 2015; Paredes-Santos et al 2013; Paredes-Santos et al,2018) tachyzoites and
797 encysted bradyzoites using methods described earlier (McPhillie et al, 2016) . We found a number
798 of these compounds including JAG21 were highly effective against tachyzoites (RH-YFP;
799 Fomovska et al, 2012) (**Figs. 1A, 2A,C**) and bradyzoites of EGS (McPhillie et al, 2016; Vidigal
800 et al, 2015; Paredes-Santos et al 2013; Paredes-Santos et al,2018) (**Fig 2B)**. For example, in a
801 separate experiment (data not shown) using immunofluorescence microscopy, the following forms
802 were observed: "true cysts" with a dolichos-staining wall, "pseudocysts" or tight clusters of
803 parasites, and small organisms. If there were fewer than four parasites visible in a cluster,
804 organisms were counted individually (as "small organisms"). A statistically significant reduction
805 in the number of true cysts and small organisms was observed at 1 μM and 10 μM for both
806 compounds ($p <0.05$, $p<0.005$). 500nM JAG21 treatment results in cultures where we do not see
807 EGS bradyzoites (e.g., **Fig. 2B**).
808
809 Results against *P. falciparum* using methodology described earlier (McPhillie et al, 2016,Trager
810 et al, 2005, Ploufe et al,2008, Johnson et al, 2007) also are shown in **Fig. 2D**. JAG 21 is potent

811 against *P. falciparum* with IC50 values ranging from 14-61 nM against a variety of drug sensitive
812 and resistant strains (McPhillie et al 2016) including D6, TM91-C235, W2, and C2B. The D6
813 strain is a drug sensitive strain from Sierra Leone, the TM91-C235 strain is a multi-drug resistant
814 strain from Thailand, the W2 strain is a chloroquine resistant strain from Thailand, and the C2B
815 strain is a multi-drug resistant strain resistant to atovaquone. Effects of other comparison
816 compounds are also shown in this table and range from 31 to 20,000 nM (**Fig. 2D**).
817
818 **ADMET superiority of JAG21**
819 *In vitro* absorption, distribution, metabolism, excretion, and toxicity (ADMET) analyses of the
820 THQ compounds were outsourced to ChemPartner Shanghai Ltd. ELQ-271 (synthesized in-house)
821 was tested as a comparison. THQs which were potent inhibitors of *T. gondii* tachyzoites were
822 assessed for their kinetic solubility, metabolic stability in human and mouse liver microsomes **(Fig.**
823 **2E)**, hERG, and their ability to permeate across MDCK-MDR1 cell membranes (*in vitro* measure
824 of blood-brain barrier (BBB) penetration potential/permeability). Solubility, half-life, HERG, and
825 BBB permeability/efflux results are shown in **Fig. 2F**. The aqueous solubility (PBS, pH 7.4) of
826 amorphous compounds JAG021 and JAG050 was 7 and 16 µM respectively, which is improved
827 over MJM170 (2 µM) and ELQ-271 (0.2 µM). We also tested solubility of the microcrystalline
828 form of JAG21 and found that the solubility was 3.5 µM. JAG021 was the most metabolically
829 stable compound in human liver microsomes (>99% remaining after 45 mins) compared with other
830 THQs and ELQ-271, although it displayed a much shorter half-life of 101 mins in mouse liver
831 microsomes. All THQs tested in the MDCK-MDR1 system for blood brain barrier (BBB)
832 permeability (including MJM170, JAG021 and JAG050), exhibited high permeability (P_{app} >10 x
833 10^6 cm/s) and low efflux (efflux ratio <1.5).
834
835 **THQs potently inhibit parasite Cytochrome bc1 (Cytbc1*)* enzyme activity**
836 JAG21 is the most active of the initially tested THQs against *T. gondii* Cytbc1*,* which also showed
837 selectivity for the parasite over the mammalian mitochondrial membrane potential (**Fig. 3**).
838 Following the full SAR testing *in vitro* activity against tachyzoites, the full set of compounds was
839 tested against HFF; then the initial compounds also were tested against the *T.gondii* and HFF
840 enzyme benchmarked against atovaquone, and ultimately the full set of compounds was compared
841 for effect against the *T. gondii* and HFF enzymes.
842
843 Mitochondrial membrane potential measurements were performed with permeabilized *T.gondii*
844 tachyzoites in suspension using safranin O, which loads into polarized membranes (see Materials
845 and Methods in the supplemental materials [Vercesi,1998]). *T. gondii* tachyzoites were
846 permeabilized with digitonin to allow the mitochondrial substrate succinate to cross the membrane
847 and energize the mitochondrion. The fluorescence of safranin O, which loads into energized
848 mitochondria was used to measure the membrane potential. The energized state of the
849 mitochondrion is observed by a decrease in fluorescence (**Figs. 3A, C, E**). Trifluoromethoxy
850 carbonylcyanide phenylhydrazone (FCCP) was used to depolarize the membrane, which causes
851 the fluorescence to go up as shown in **Fig. 3A**. JAG21 depolarized the membrane potential even
852 at concentrations as low as 2 nM (**Fig. 3C, D**). JAG21 and Atovaquone had similar effects on the
853 mitochondrial membrane potential **(Fig. 3D)**.. **Fig. 3F** is host cells so indicates that it is less toxic.
854 Other compounds like JAG46 and 47 showed almost no effect at doses as high as 4 µM (**Fig.**
855 **3A,B**). JAG50 showed depolarizing activity at doses of 200 nM and higher. The effect of these
856 THQ compounds against the *T. gondii* mitochondrial membrane potential was greater than the
857 effect on the human foreskin fibroblast membrane potential (**Fig. 3E,F**). This is consistent with
858 the observation that JAG21 is less toxic against human Telomerase reverse transcriptase

immortalized (hTERT) HFF cells than atovaquone. We had newly created THQ compounds, not yet characterized fully, that show even less toxicity to the human fibroblast cytochrome b/c complex marked with ** in **Fig 1A**. These could be developed in a second phase of our program were reductions in toxicity needed. However, as data presented herein demonstrates, there are significant advantages in the ADMET properties of JAG 21, and its dramatic efficacy *in vivo,* without toxicity. There may be no need to further develop any of those potential additional leads.

Enzyme reduction of cytochrome *c* by *P. falciparum* parasite extract (Fisher et al, 2004, 2009) is mediated by *P. falciparum* bc_1 complex cytochrome *c* reductase ($Pfbc_1$) enzyme. All three compounds tested (1 μM) significantly inhibited the reduction of cytochrome *c* by the *P. falciparum* parasite extract, (JAG021 = 86.4 ± 3.2; JAG099 = 81.3 ± 6.0; MJM170 = 69.7 ±11.3 % of the atovaquone response, **Fig. 3G**. Additional data demonstrated selective effect on *P. falciparum* enzyme compared with bovine enzyme (data not shown).

Binding, Co-crystallography, Pharmacophore and Co-Cryo-Electron Microscopy Studies Demonstrate Selectivity

In binding assays and in co-crystallography (McPhillie et al, 2016; Capper et al ,2015; Amporndanai et al, 2018; Battye et al, 2011; Emsley et al, 2010; Laskowski and Swindells, 2011;Lbebedev et al, 2012; Murshudov et al, 2011; Emsley et al, 2004; Zheng et al, 2017; Zhang et al, 2016), JAG021 has lower binding affinity to bovine cytochrome *bc* in comparison with previous compounds that we have tested. JAG 21 'inhibits' Cyt*bc1* but not fully, indicating that it will be less toxic for mammalian (bovine/human) cyt *bc1* than the apicomplexan enzymes (**Fig. 4A**). The electron density map in the Qi site of bovine cytochrome bc_1 complex with JAG021 **(Table S1,** Data Collection Statistics)**)** reveals an additional electron density, which allowed unambiguous positioning of the inhibitor (**Fig. 4B**). No additional electron density was found within the Q_o site. After the refinement, $2F_o$-F_c electron around JAG021 becomes clearer (**Fig. 4C)**. The second aromatic ring in the tail group of the compound is less defined due to high flexibility introduced by the oxygen linker. The quinolone head of JAG021 is held between Asp228 and His201 and adapted the same conformation as 4(1H)-pyridone (GSK932121)(Capper et al, 2015) (**Fig. 4D**) and tetrahydro-4(1H)-quinolone (MJM170) (McPhillie et al, 2016) (**Fig. 4E**) by directing the NH group to His201 and the carbonyl group to Asp228. The carbonyl of the quinolone head and OG1 atom of Ser35 are within 3.0 Å distance that allows hydrogen bonding and enhances the binding affinity to the bovine enzyme. The 3-diarylether tail extends along a hydrophobic channel defined by Gly38, Ile39 and Ile42. The trifluoromethoxy group at the phenoxy ring points towards Met190 and Met194 (**Fig. 4F**). CryoEM studies of the complex also demonstrates reasons for selectivity. In **Fig. 4F**, the density suggests that the inhibitor can adopt two different binding poses as observed previously in the cryo-EM structure of GSK932121(Capper et al, 2015). The binding pose shown in yellow, which has the strongest density, agrees with the crystal structure and has the trifluoromethoxy group pointing towards Met194. However, there is additional density which could result from a second binding pose (green) in which the trifluoromethoxy group points towards Asp228(McPhillie, 2016 et al)**. Fig. 4F,** shows GSK932121 pyridone (PDB:4D6U) (**G**) MJM170 quinolone (PDB:5NMI).

JAG21 is potent *in vivo*

In vivo studies of JAG21 against *T. gondii* demonstrated high efficacy in a variety of settings. JAG21 at 5 mg/kg/day administered IP improves well-being and eliminates illness and *T. gondii* Type II Prugneaud luciferase tachyzoites completely in luminescence studies (**Fig. 5A**). Further,

907 treatment beginning on day one after infection results in no cysts being found in brains of these
908 mice treated for 14 days with 5mg/kg/day of JAG21, when brains were evaluated 30 days after
909 stopping JAG21 treatment in two replicate experiments. Treatment beginning on day 30 after
910 initiation of infection with Type II Me49 parasites results in marked, statistically significant
911 reduction in normal appearing cysts, free organisms and immunoperoxidase stained cysts detected
912 by automated imaging of scanned slides (**Figs. 5 B,C**, $p<0.03$ experiment ; $p<0.01$ experiments 1
913 and 2 together, **Supplemental Fig.S1**). The automated analysis confirmed results from the blinded
914 microscopic visual quantitation of cysts and free organisms in slides by two observers. Adding
915 tafenoquine or primaquine to treatments of active plus dormant malarias(St.Jean et al, 2016;
916 Lacerda et al, 2019; Llanos-Cuentas et al 2019) is partially effective against both active and
917 dormant phase plasmodia, when neither treatment of active nor dormant disease alone is effective
918 for either *in vivo*. We developed experiments based on these observations where experiments with
919 tafenoquine alone or with JAG21 alone was used in the experiments with established cyst with
920 immune competent mice. This was to determine whether tafenoquine might add to efficacy of
921 JAG21. The efficacy of treatment with JAG21 alone was so robust (**Fig. 5B**), that no additive
922 effect was seen, or could have been detected, by adding Tafenoquine to JAG21. Efficacy was
923 shown when data were analyzed as separate groups, i.e., control vs JAG21 alone ($p<0.03$) or
924 control vs JAG21 plus tafenoquine, or grouping the JAG21 and JAG21 plus tafenoquine results as
925 "untreated" versus "treated" ($p<0.01$). Analysis shown combining both treatment groups from two
926 replicate experiments showed similar results ($p<0.01$).(**Fig 5B**), and when results from replicate
927 experiments were grouped(Supplemental **Fig S1**). In **Fig 5C** the control mice had cysts with usual
928 morphology (Top two panels), whereas treated mice had very few morphologically recognizable
929 usual cysts that were immunostained (bottom panels).
930 A nano formulation homogenized (<6 μM) was used effectively orally for the *P.bergheii*
931 experiments, further, importantly, was effective in the single oral dose causal prophylaxis in 5
932 C57BL/6 albino mice at 2.5 mg/kg dosed on day 0, 1 hour after intravenous administration of
933 10,000 *P. berghei* sporozoites was completely protective. In addition, 3 dose causal prophylaxis
934 treatment in 5 C57BL/6 albino mice at 0.625 mg/kg dosed on days -1, 0, and +1 also was
935 completely protective. A representative experiment at a higher dose (5 mg/kg) is shown, but all
936 experiments with the oral dosing regimen with the nanoformulation specified above showed 100%
937 survival 30 days post infection with *P. berghei*, where all liver and blood stage parasites were
938 eliminated (**Fig. 5D,E)** demonstrates not only efficacy of JAG21 against the three life cycle stages
939 of *P. berghei*, but also demonstrates the efficacy of oral administration of the nanoformulation
940 when used immediatel, at a low dose.
941
942 **G1 Arrest, Persisters, Companion Compounds**

943 In mice that were treated with JAG21 early after infection (**Fig 5A**) we could find no residual
944 immunostaining for *T.gondii* in brain tissue of any mice. This suggests that very early treatment
945 could prevent established, chronic infection, for example in epidemics such as those that occurred
946 in Victoria, Canada, the U.S.A., and Brazil. In mice with established cysts, following treatment
947 with JAG21, we occasionally saw a small number of cysts (**Fig 5B**) and amorphous immunostained
948 structures (**Fig. 5C** bottom panels). This was reminiscent of persistence in some malaria infections
949 (Cubi et al, 2017) and abnormal immunostained structures we previously identified with a
950 conditional, tetracycline-on regulatable, mutant *T.gondii* (Hutson et al, 2010 and Fog.S2). In this
951 ΔRPS*13* tachyzoite, small ribosomal protein 13 can be regulated, depending on whether
952 anhydrotetracycline (ATc) is absent or present, leading the ATc responsive repressor to be on or

953 off response elements engineered into the promoter (Hutson et al, 2010). ΔRPS*13* replicates with
954 ATc present and is arrested in G1 when ATc is absent in HFF cultures (Hutson et al 2010). The
955 dormant parasite could persist for extended periods (Hutson et al, 2010). The parasite could be
956 rescued from its dormant – ATc state by adding ATc, months after removing tetracycline from
957 infected HFF cultures, although it could not be rescued in immunocompetent mice with LNAME
958 and ATc when tested one week after infection (Hutson et al 2010). We wondered if this type of
959 dormant organism could form *in vivo*, whether it could contribute in a biologically relevant way
960 to dormancy and recrudescence, similar to the malaria hypnozoite, and whether JAG 21 might be
961 able to eliminate it, or whether a companion compound effective against this form might be needed
962 or work in conjunction with JAG21 if needed. To begin to address these questions and to
963 investigate how close the *T. gondii* ΔRPS*13* -ATc phenotype might be to the malaria hypnozoite,
964 we compared the transcriptome of *T. gondii* ΔRPS*13* in human, primary, brain, neuronal stem cells
965 +/-ATc to the recently published *P. cynomolgi* hypnozoite transcriptome established with single
966 cell RNA sequencing in laser captured organisms (Cubi et al, 2017). This analysis identified 28
967 orthologous genes with similar expression pattern in both *T. gondii* ΔRPS*13* -ATc and *P.*
968 *cynomolgi* hypnozoites, including the downregulation of rps*13* and upregulation of the eukaryotic
969 initiation factor-2α kinase IF2K-B, a protein involved in translational control in response to stress
970 (Cubi et al 2017) (**Fig 6A**). Further. assessment of the *T. gondii* ΔRPS*13* transcriptome in the
971 absence or presence of ATc showed upregulation of additional IF2K members, 25 Apetela (AP) 2
972 transcription factors and a number of genes that participate as protein ubiquitin ligases, and in
973 trafficking as well as in RNA binding (**Supplemental Table S2**). None of them, except for
974 AP2VIIa-7, have been shown to be upregulated nor downregulated during differentiation to
975 bradyzoites. Gene set enrichment analysis showed that in the absence of ATc, the *T. gondii*
976 ΔRPS*13* transcriptome is enriched in genes typically expressed during G1, confirming previous
977 results indicating that downregulation of *rps13* arrests the parasite at this stage of the cell cycle
978 (**Fig. 6B**) (Hutson et al, 2010). Moreover, a number of biological processes are downregulated
979 without ATc, including protein synthesis and degradation as well as energy metabolism (**Fig. 6B**).
980 Noteworthy, some gene ontology (GO) terms enriched in *T. gondii* ΔRPS*13* -Tc are also
981 overrepresented in the *P. cynomolgi* hypnozoite (stars in **Fig. 6D**). Further, without ATc the
982 transcriptome of *T. gondii* ΔRPS*13* is compatible with a parasite transitioning from an active
983 replicating form to a dormant stage, reflected by the downregulation of genes typical of the S and
984 M stages of the cell cycle, and of genes that participate in energy metabolism and virulence (**Fig.**
985 **6B, D**, and **Supplemental Table S2 and Fig S2**). It has been reported that with treatment of active
986 forms of malaria, hypnozoites still persist, and recrudesce later (Cubi et al, 2017, Hutson et al
987 2010; St.Jean et al, 2016; Lacerda et al, 2019; Llanos-Cuentas et al, 2019). Also, compounds that
988 target cytochrome b/c were not effective against malaria hypnozoites. If primaquine or
989 tafenoquine, which do not treat the active *P.vivax* parasites, were added *in vivo,* hypnozoites have
990 been shown not to recrudesce, or do so less often (St. Jean et al, 2016; Lacerda et al, 2019; Llanos-
991 Cuentas et al,2019). Testing with primaquine or tafenoquine could only be performed *in vivo,* as
992 activity against the hypnozoite requires hepatic metabolism of primaquine or tafenoquine (St.J ean
993 et al 2016;Lacerda et al, 2019; Llanos-Cuentas et al,2019). Tafenoquine is not active in tissue
994 culture which is consistent with the findings that these compounds require hepatic metabolism. To
995 establish a parallel *in vivo* system, we studied immune compromised mice (Interferon ϒ receptor
996 knockout mice with the knockout in the germline) infected with ΔRPS*13* herein. Although in
997 immune competent mice ΔRPS*13* does not recrudesce with ATc treatment beyond 3 days after
998 infection, we found that when ATc was added after treatment of the immune compromised mice

with JAG21 dosed intraperitoneally for 14 days, the dormant ΔRPS*13* parasite could still recrudesce after JAG21 treatment was discontinued and tetracycline added (**Fig. 6C, Supplemental Fig. S2**). Consistent with adding tafenoquine to treatment of *P.vivax* malaria with chloroquine where both medicines together were partially effective against the active and hypnozoite forms, the combination of JAG21 and tafenoquine had a modest effect together on transiently improving survival time when ATc was added when compared with JAG21 or tafenoquine alone (**Fig 6C, Supplemental Fig. S2**). The trend in the result seems similar to the malaria infections where hypnozoites form, although protection was not as robust, as in the malaria model, and we did not achieve complete, durable protection against ΔRPS*13*. **These results in Figures 6C and S2 suggest:** a. In G1 arrested organisms that begin as tachyzoites, they can persist *in vivo* even if their morphology as parasites is difficult to discern; b. Treatment with JAG21+Tafenoquine can prolong time to death more robustly than other treatments; c. But, in these immune compromised mice at this dosage regimen this treatment did not robustly, durably protect these mice from death later; d. In these immune compromised mice, whether this lack of complete protection was because of immune compromise, or less than optimal duration of treatment, or suboptimal dose or timing of treatments, or that this G1 arrested organism is harder to treat, remains to be determined in future studies. The modest efficacy of the two compounds, administered together, suggests that treating both tachyzoites and the G1 arrested organisms is important. This seems similar to *P. cynomogli* and *P. vivax* treatment with tafenoquine and chloroquine studies, which also showed efficacy but was not completely successful in preventing relapse. At the time this study was performed, formulation and dosing (including duration and timing) had not yet been optimized formally for the *T.gondii* model. *P. vivax* treatment requires chloroquine to treat blood schizonts and tafenoquine to treat hypnozoites. Treatment in man, per the FDA approved label, consists of a single dose of 300 mg on day 1 co-administered with chloroquine treatment on days 1 or 2. Both medicines have long half-lives in humans. This treatment was relatively effective in humans, with about a 30% recurrence rate.

Sinai et al have demonstrated heterogeneity in the phenotypes of organisms within established cysts. Their work found bradyzoites within cysts are not uniform with regard to their replication potential (Watts et al, 2015), mitochondrial activity (Sinai, unpublished), and levels of the glucose storage polymer amylopectin (Sinai, unpublished). These properties of bradyzoites within (Watts, et al, 2015), and properties of tissue cysts vary during the course of infection with unappreciated levels of complexity in the progression of chronic toxoplasmosis (Watts et al, 2015). The analysis (**Fig 6D**) of the ΔRPS*13* infected NSC suggests molecular targets modified in this G1 arrested ΔRPS*13* parasite as shown in **Fig 6D** Supplemental **Table S2**. In the future, with formulation and pharmacokinetics of JAG21 optimized, it will be of interest to determine whether JAG21 can eliminate these organisms and any residual structures as in **Fig6C,** or whether adding synergistic compounds such as atovaquone (**Fig 4B**) or antisense effective against these upregulated molecular targets, such as kinases, ATPases, AP2s (**Fig 6D and Table S2**), or a newly recognized bradyzoite master regulator of differentiation might be effective alone or might be synergistic with JAG21 against this ΔRPS*13*, as well as the conventional recognized tachyzoite and bradyzoite life cycle stages. Chen et al reported in the transcriptomes of established bradyzoite *in vivo* cysts that EIF2kinase of stressed parasites is present (Chen et al, 2018), but we have not found other overlap of Chen's transciptome with *P cynomogoli* or ΔRPS*13* transcriptomes. Others have described EIF2kinase and stress granules only in transitioning or extracellular parasites (Watts et al, 2015). Bradyzoites within tissue cysts are not monolithic, so in future studies single cell RNA sequencing of bradyzoites obtained by laser capture of bradyzoites *in vivo* defined on the basis of their

physiological state, may be needed to determine whether a transcriptome signature similar to ΔRPS*13* is sometimes present, linked to morphologic/immunostaining features that might functionally distinguish them to define the character of a hypnozoite-like state in *T.gondii*. We noted hererogeneity of parasite phenotype, even in the same vacuoles In our earlier IFA and electron microscopic characterization of G1 arrested ΔRPS*13* in HFF (Hutson et al, 2010). Heterogeneity also was found very recently in tachyzoites and bradyzoites created by alkaline conditions in culture across the cell cycle *in vitro* in HFF, using single cell RNA sequencing (Xue et al Biorx, 6/3/2019 In Press). These authors also noted that what had been interpreted as "noise" earlier was found actually to be signal in a more complex environment. These authors suggest that such heterogeneity might make developing curative treatments more complex. Our analysis of JAG21 effects and the ΔRPS*13*-ATet knockdown herein begin to help address this question: We noted that consistent with heterogeneity in our IFAs, in our comparison with the Xue et al's heterogeneous P1-6 clusters analysis, we found that most of the up- or down-regulated genes are within P3-P5 tachyzoite clusters. Also, consistent with the heterogeneity we observed in our G1 arrested ΔRPS*13* -ATet comparison, ΔRPS*13* has a drop in SAG1 and elevated SRS44 that is consistent with a brady-like phenotype. BAG1 expression was too low overall to draw any conclusion about BAG1. It is also noteworthy that in our -ATet relative to +Atet conditions in primary, human, brain, neuronal stem cells, the master regulator of bradyzoite differentiation is slightly overexpressed (Log_2 Fold Change=0.7, adjusted p-value=0.043). Although JAG21 is highly potent against tachyzoites and bradyzoites, it did not eliminate every long-established encysted bradyzoite or -ATet ΔRPS*13* completely either *in vitro* or in IFNγ knock-out mice *in vivo*. Consistent with heterogeneity, herein JAG21 treatment of *Δ*RPS*13* and transcriptomics analyses define a metabolically quiescent, persister,"stasis" state that is reversible even after substantial periods of dormancy, that contribute to conceptual and functional understanding of both Plasmodia species and *T. gondii* infections and molecular mechanisms whereby "persisters" might be eliminated.

An oral nanoformulation is potent against virulent RH

To further develop JAG21 for practical, clinical use, our next step was to make a formulation that is stable at room temperature, and would be effective when administered orally: Following a number of unsuccessful alternative methods (data not shown, a dispersion of JAG21 was prepared using hydroxyethyl cellulose (HEC) and Tween 80. This new formulation method is described in the Materials and Methods. When this dispersion was imaged using a Nikon ECLIPSE E200 optical microscope set to 40x magnification, the average particle size of the JAG21 dispersion in HEC/Tween 80 was determined using an in-house image analysis program and was found to be 2.85µm (**Fig. 7A**). Material was re-sonciated the same way just prior to administration after being stored for 6 months and retained the same properties (**Fig 7A**) when imaged. Following administration of 2,000 highly virulent RH Strain tachyzoites intraperitoneally, the oral nanoformulation was administered by gavage using a 21 gauge needle. This was given either (1) as a single dose of 5, 10, or 20mg/kg, or (2) three daily doses of 10mg/kg given for the first three days after infection. After 5 days the RH strain tachyzoites in peritoneal fluid of each mouse were quantitated by measurement of YFP they expressed using a flurimeter and by quantitating parasites present in peritoneal fluid using a hemocytometer. Parasite burden was reduced by ~60% 5 days later following the single doses of 10 and 20mg/kg (representative experiment with 10mg/kg shown in **Fig.7B**; $p<0.03$) and markedly reduced with three doses of 10mg/kg administered on each of the first three days after intraperitoneal injection of the virulent RH strain tachyzoites

(**Fig.7C**, representative experiment, p<0.001). This is the proof of principle that will facilitate media milling, dispersant, and a self disintegrating tablet in the future. JAG21 has real promise as a mature lead compound to treat both *T.gondii* and Plasmodium species infections.

DISCUSSION

T.gondii infections are highly prevalent and the impact of this disease can be devastatingly severe. Current treatments have toxicity or hypersensitivity side effects. New compounds that are without toxicity or hypersensitivity, and that are highly active against tachyzoites would be of considerable clinical usefulness. Further, no medicines are active against the encysted stage or definitively curative. In addition, malaria is lethal for 1 child every eleven seconds and a threat to travelers going to endemic areas. Development of drug resistance also increases the need for new anti-malarial compounds. Our goal in this work herein was to identify compounds highly effective against *T . gondii* and *P. falciparum*, and we believe we have achieved our goal by developing lead compounds with dual activity.

To further develop the THQ series, 54 compounds were synthesized to improve kinetic solubility, solubility in physiologically-relevant media (FaSSIF, FeSSIF), and metabolic stability (microsomes and hepatocytes), and other ADMET properties. Compounds JAG050 and JAG021 were identified as lead compounds, demonstrating potent inhibition on both tachyzoites and bradyzoites life stages and were not toxic to human cells in our *in vitro* model (HFF). In addition, both compounds displayed low nanomolar efficacy against multiple drug resistant strains of *P. falciparum in vitro.* JAG050 and JAG021 demonstrate promising ADMET properties, with JAG21 slight superior due to the compound's longer metabolic stability in human and mouse microsomes.

A striking result with JAG21 in our *in vivo* parasite studies is the compound's high efficacy against *T.gondii* tachyzoites and bradyzoites. In our *P. berghei in viv*o model for malaria, we observed that a single dose causal prophylaxis in 5 C57BL/6 albino mice at 2.5 mpk dosed on day 0, 1 hour after intravenous administration of 10,000 *P. berghei* sporozoites was achieved. Causal prophylaxis was also observed after a 3-dose treatment in 5 C57BL/6 albino mice at 0.6 mpk dosed on days -1, 0, and +1. A representative figure at a higher dose (5 mg/kg) is shown, and all experiments with the amounts mentioned above demonstrated identical high efficacy in luminescence, parasitemia, and survival results. This demonstrates that JAG21 functions better in this *in vivo* model than the ELQ 300 series where prodrug formulation is required to achieve solubility and efficacy In contrast to the efficacy of JAG21 at 2.5mg/kg in a single oral dose model resulting in cure without a prodrug. ELQ 300 (not the prodrug) was not effective at doses between 1 and 20 mg/kg although the prodrug was more effective (Doggett, et al 2012); Freuh et al, 2017).

JAG050 and JAG021 are lead compounds, with JAG21 being a superior compound due to its favorable predicted ADMET properties, potency, efficacy and lack of toxicity. JAG021 demonstrates increased solubility and potential for advanced formulation. There also is potential for improving solubility and reducing toxicity further because of the larger binding pocket in the apicomplexan Cytbc1 enzyme compared with the mammalian Cytbc1 enzyme, determined by modeling occupancy of the structure, enzyme assays and empirically, if it were needed. We have created and tested additional compounds that take advantage of these properties, although none at present, have the proven ADMET and marked *in vivo* efficacy we found to be advantages in our proof of principle studies of JAG21. At present, however, our mature lead compound has sufficient drug like properties to move to advanced formulations, suggesting increased bulk will not be needed to reduce toxicity. It has selectivity as demonstrated by our enzymatic, binding and

structure studies, although there are additional compounds that show even greater selectivity. It is highly effective in an oral nano preparation against *P. berghei* three life cycle stages, and with early treatment appears to be capable of curing toxoplasmosis in immunocompetent mice. This work demonstrates the promising nature of this novel tetrahydroquinolone scaffold and mature lead compound. JAG21 has the potential to become an orally administered medicine or with partners, part of a medicine combination that is curative for toxoplasmosis and is a single dose cure for malaria. It is suitable for partnering with other compounds to obviate problems with selection of resistant mutants. We have demonstrated earlier that the parent compound with this new scaffold is synergistic with atovaquone and additive with cycloguanil (in proguanil) against *P. falciparum* (McPhillie et al, 2016). This compound is a mature lead compound to treat both *T.gondii* and Plasmodium species infections. If utility and safety is retained and no toxicity appears in next stage studies, this compound may become suitable for treatment of *T. gondii* and *P. falciparum* infections.

CONCLUSION

JAG21 has real promise as a mature lead compound to treat both *T.gondii* and Plasmodium species infections, demonstrated *in vitro* and *in vivo*. It has high efficacy against *T.gondii* tachyzoites and bradyzoites, and established encysted organisms. Treatment with a single low oral dose is effective for causal prophylaxis and radical cure *of P.berghei* infections. JAG 21 has complete efficacy against three life cycle stages of *P.berghei*. In terms of companion inhibitors, JAG21, a Q_i inhibitor, synergizes against tachyzoites with atovaquone (a Q_o inhibitor) *in vitro*. It appears able to contribute modestly to protection of immune compromised mice in conjunction with tafenoquine against an initially replicating, then G1 arrested, *T.gondii* parasite that shares key transcriptomic components with *P. cynomolgi* hypnozoites. Our mature lead compound has sufficient selectivity and drug-like properties to support ongoing efforts to further develop this compound through preparation of advanced formulations and testing of additional study of pharmacokinetics, efficacy and safety.

ETHICS STATEMENT

This study was carried out in accordance with regulations of The University of Chicago IACUC and IBC and of The Home Office of the UK Government under the Animals [Scientific Procedures] Act 1986. All work in the UK with mice was covered by License PPL60/4568, Treatment and Prevention of Toxoplasmosis with approval by the University of Strathclyde ethical review board.

AUTHOR CONTRIBUTIONS

Conception and Design. Overall: MMc, RMc, MH, HL, SNM, CWF, CWR, SPM, GB, SA, KR, RP, LY**; Subparts of manuscript: all authors.**
Performed Experiments and/or analyzed data. All authors.
Wrote manuscript. Overall: MMc, RMc, MH, HL**; Subparts of manuscript: all authors.**
Reviewed/Edited Manuscript in final form: All Authors
.

ACKNOWLEDGMENTS

This work was supported by NIAID NIH DMID U01 AI082180 (RMc) and the National Institute of Diabetes and Digestive and Kidney Diseases (NIDDK) Grant #5T35DK062719-28 to FE. This was also supported by National Institutes of Health (NIH) contract number HHNS272200900007C, NIH. National Institute of Allergy and Infectious Diseases of the National Institutes of Health (NIAID) award numbers R01AI071319(NIAID) and R01AI027530 (NIAID) (RMc); NIAID contract Number HHNS272200900007C; NIAID award number U19AI110819 (HL): NIAID award number U01 AI077887(NIAID) and Defense Threat Reduction Agency award number 13-C-0055, and Department of Defense award numbers W911NF-09-D0001 and W911SR-07-C0101(MH). We thank and gratefully also acknowledge the support of the Cornwell Mann family, the Ramirez, Musillami, Quinn, Rosenthal, Greenberg, Morel, Rooney and Engel families, Taking out Toxo, and The Toxoplasmosis Research Institute. The work also was supported by the Bill and Melinda Gates Foundation (BMGF, OPP1150755) (RP). This material is based upon work supported by the National Science Foundation Graduate Research Fellowship under Grant No. #DGE-1656466 awarded to K.D.R. We acknowledge the assistance of Leon Wang, PhD of Princeton University's with size determination for the final step of nanoformulation for this proof of principle study. Dennis Steindler, PhD kindly provided the primary human brain neuronal stem cells used in this study.

SUPPLEMENTARY MATERIAL

More detail for the ΔRPS*13* experiments; **Summary; Supplemental Tables S1, S2; Figures S1;S2.** Material for this article can be found online at: https://www.frontiersin.org/articles/.....

REFERENCES

Anders S, Pyl PT, Huber W. (2015) HTSeq--a Python framework to work with high-throughput sequencing data. Bioinformatics. 31(2):166-9. doi: 10.1093/bioinformatics/btu638.

Amporndanai K, Johnson RM, O'Neill PM, Fishwick CWG, Jamson AH, Rawson S et al., (2018). X-ray and cryo-EM structures of inhibitor-bound cytochrome bc 1 complexes for structure-based drug discovery. IUCrJ, 5, 200–210.

Battye TG, Kontogiannis L, Johnson O, Powell HR, Leslie AG. (2011) iMOSFLM: A new graphical interface for diffraction-image processing with MOSFLM. Acta Crystallographica Section D: Biological Crystallography, 67(4), 271–281.

Caumes E, Bocquet H, Guermonprez G, Rogeaux O, Bricaire F, Katlama C, et al. (1995) Adverse cutaneous reactions to pyrimethamine/sulfadiazine and pyrimethamine/clindamycin in patients with AIDS and toxoplasmic encephalitis. Clin Infect Dis Off Publ Infect Dis Soc Am. 21(3): 656–8.

Capper MJ, O'Neill PM, Fisher N, Strange RW, Moss D, Ward SA, et al. (2015). Antimalarial 4(1H)-pyridones bind to the Qi site of cytochrome bc1. Proceedings of the National Academy of Sciences, 112(3):755–760.

1230 Chen LF, Han XL, Li FX, Yao YY, Fang JP, Liu XJ, et al (2018) Comparative studies of
1231 Toxoplasma gondii transcriptomes: insights into stage conversion based on gene expression
1232 profiling and alternative splicing. Parasites and Vectors 11:402
1233
1234 Croken MM, Qiu W, White MW, Kim K. (2014) Gene Set Enrichment Analysis (GSEA) of
1235 Toxoplasma gondii expression datasets links cell cycle progression and the bradyzoite
1236 developmental program. BMC genomics. 15:515. doi: 10.1186/1471-2164-15-515.
1237
1238 Cubi R, Vembar SS, Biton A, Franetich JF, Bordessoulles M, Sossau D, et al (2017) Laser capture
1239 microdissection enables transcriptomic analysis of dividing and quiescent liver stages of
1240 Plasmodium relapsing species. P cynomogoli Cell Microbiol. 19(8). doi: 10.1111/cmi.12735.
1241
1242 Delair E, Latkany P, Noble AG, Rabiah P, McLeod R, Brézin A. (2011) Clinical manifestations
1243 of ocular toxoplasmosis. Ocul Immunol Inflamm. 19(2):91-102. doi: 10.3109/09273948.2011.
1244 564068.
1245
1246 Doggett JS, Nilsen A, Forquer I, Wegmann KW, Jones-Brando L, Yolken RH, et al. (2012)
1247 Endochin-like quinolones are highly efficacious against acute and latent experimental
1248 toxoplasmosis. Proc Natl Acad Sci U S A. 109(39):15936–41.
1249
1250 Emsley P; Cowtan K (2004). Coot: model building tools for molcular graphics. Acta Cryst. D60,
1251 2126-2132 doi:10.1 107/S0907444904019158
1252
1253 Emsley P. Lohkamp,B. Scott, W.G. Cowtan,K. (2010). Features and Development of Coot. Acta
1254 Crystallographica. D66: 486–501.
1255
1256 Evans, PR., (2011). An introduction to data reduction: Space-group determination, scaling and
1257 intensity statistics. Acta Crystallographica Section D: Biological Crystallography, 67(4), 282–292.
1258
1259 Fisher N. Warman A. Ward SA. Biagini GA (2009). Chapter 17 Type II NADH: Quinone
1260 Oxidoreductases of Plasmodium Falciparum and Mycobacterium Tuberculosis: Kinetic and High-
1261 Throughput Assays. Methods in Enzymology, ed. Mitochondrial Function, Part A: Mitochondrial
1262 Electron Transport Complexes and Reactive Oxygen Species. 456: 303–320.
1263
1264 Fisher N, Castleden CK, Bourges I, Brasseur G, Dujardin G, Meunier B (2004). Human disease-
1265 related mutations in cytochrome b studied in yeast. The Journal of biological chemistry, 279(13),
1266 12951–12958.
1267
1268 Fomovska A, Wood RD, Mui E, Dubey JP, Ferreira LR, Hickman MR, et al. (2012) Salicylanilide
1269 inhibitors of Toxoplasma gondii. J Med Chem. 55(19): 8375–91
1270
1271 Fomovska A, Huang Q, El Bissati K, Mui EJ, Witola WH, Cheng G, et al. (2012a) Novel N-
1272 Benzoyl-2-Hydroxybenzamide Disrupts Unique Parasite Secretory Pathway. Antimicrob Agents
1273 Chemother [Internet]. 56(5):2666–82.
1274

1275 Frueh L, Li Y, Mather M, Li Q, Pou S, Nilsen A, et al (2017). Alkoxycarbonate Ester Prodrugs of
1276 Preclinical Drug Candidate ELQ-300 for Prophylaxis and Treatment of Malaria. ACS Infect. Dis.,
1277 DOI: 10.1021/acsinfecdis.7b00062
1278
1279 Gubbels M-J, Li C, Striepen B. (2003) High-Throughput Growth Assay for Toxoplasma gondii
1280 Using Yellow Fluorescent Protein. Antimicrob Agents Chemother 47(1):309-16
1281
1282 Hutson SL, Mui E, Kinsley K, Witola WH, Behnke MS, El Bissati K, et al (2010) T. gondii RP
1283 promoters & knockdown reveal molecular pathways associated with proliferation and cell-cycle
1284 arrest. PLoS One. 5(11):e14057. doi: 10.1371/journal.pone.0014057.
1285
1286 Johnson JD, Dennull RA, Gerena L, Lopez-Sanchez M, Roncal NE, Waters NC. (2007)
1287 Assessment and Continued Validation of the Malaria SYBR Green I-Based Fluorescence Assay
1288 for Use in Malaria Drug Screening. Antimicrob Agents Chemother 51:1926–1933.
1289
1290 Kim D, Langmead B, Salzberg SL. (2015) HISAT: a fast spliced aligner with low memory
1291 requirements. Nature methods. 12(4):357-60. doi: 10.1038/nmeth.3317.
1292
1293 Khan AA, Nasr M, Araujo FG. (1998) Two 2-hydroxy-3-alkyl-1,4-naphthoquinones with in vitro
1294 and in vivo activities against Toxoplasma gondii. Antimicrob Agents Chemother. 42(9): 2284–9.
1295
1296 Lacerda MVG, Llanos-Cuentas A, Krudsood S, Lon C, Saunders DL, Mohammed R, et al. (2019)
1297 Single-dose Tafenoquine to Prevent Relapse of Plasmodium vivax Malaria. N Engl J Med 380:
1298 215-28.
1299
1300 Laskowski, RA. Swindells, M.B., (2011). LigPlot +: Multiple Ligand À Protein Interaction
1301 Diagrams for Drug Discovery. journal of chemical information and modeling, 51: 2778–2786.
1302
1303 Lebedev, AA et al., (2012). JLigand: A graphical tool for the CCP4 template-restraint library. Acta
1304 Crystallographica Section D: Biological Crystallography, 68(4): 431–440.
1305
1306 Llanos-Cuentas A, Lacerda MVG, Hien TT, Vélez ID, Namaik-Larp C, Chu CS, et al. (2019)
1307 Tafenoquine versus Primaquine to Prevent Relapse of Plasmodium vivax Malaria N Engl J Med
1308 380:229-41
1309
1310 Love MI, Huber W, Anders S. (2014) Moderated estimation of fold change and dispersion for
1311 RNA-seq data with DESeq2. Genome biology. 15(12):550. doi: 10.1186/s13059-014-0550-8.
1312
1313 Lykins J, Wang K, Wheeler K, Clouser F, Dixon A, El Bissati K, et al (2016) Understanding
1314 Toxoplasmosis in the United States Through "Large Data" Analyses. Clin Infect Dis. 63(4):468-
1315 75. doi: 10.1093/cid/ciw356.
1316
1317 Marcsisin SR, Sousa JC, Reichard GA, Caridha D, Zeng Q, Roncal N, et al (2014) Tafenoquine
1318 and NPC-1161B require CYP 2D metabolism for anti-malarial activity: implications for the 8-
1319 aminoquinoline class of anti-malarial compounds. Malar J. 13:2. doi: 10.1186/1475-2875-13-2
1320

McLeod R, Khan AR, Noble GA, Latkany P, Jalbrzikowski J, Boyer K. (2006) Severe sulfadiazine hypersensitivity in a child with reactivated congential toxoplasmic chorioretinitis. Pediatr Infect Dis J. 25(3):270-2.

McLeod R, Boyer K. (2018) Toxoplasmosis (Toxoplasma gondii). In: Nelson Textbook of Pediatrics. 21st ed. Elsevier.

McPhillie M, Zhou Y, El Bissati K, Dubey J, Lorenzi H, Capper M, et al (2016) New paradigms for understanding and step changes in treating active and chronic, persistent apicomplexan infections. Sci Rep. 6:29179. doi: 10.1038/srep29179.

Miley GP, Pou S, Winter R, Nilsen A, Li Y, Kelly JX, et al (2015) ELQ-300 Prodrugs for Enhanced Delivery and Single-Dose Cure of Malaria AAC 59: 5555-556

Muller I, Jex AR, Kappe SHI, Mikolajczak SA, Sattabongkot J, Patrapuvich R, et al Vivax sporozoite consortium. (2019) Transcriptome and histone 1 epigenome of Plasmodium vivax salivary-gland sporozoites point to tight regulatory control and potential mechanisms for liver-stage differentiation. Int J Parasitol 49(7):501-513

Muench SP, Prigge ST, McLeod R, Rafferty JB, Kirisits MJ, Roberts CW, et al (2007) Studies of Toxoplasma gondii and Plasmodium falciparum enoyl acyl carrier protein reductase and implications for the development of antiparasitic agents.Acta Crystallogr D Biol Crystallogr. 63(Pt 3):328-38.

Murshudov GN, Skubák P, Lebedev AA, Pannu NS, Steiner RA, Nicholls RA, et al., (2011). REFMAC5 for the refinement of macromolecular crystal structures. Acta Crystallographica Section D: Biological Crystallography, 67(4): 355–367.

Ngô HM, Zhou Y, Lorenzi H, Wang K, Kim TK, Zhou Y, et al (2017) Toxoplasma Modulates Signature Pathways of Human Epilepsy, Neurodegeneration & Cancer. Sci Rep. 7(1):11496. doi: 10.1038/s41598-017-10675-6.

Paredes-Santos TC, Martins-Duarte ES, Vitor RW, de Souza W, Attias M, Vommaro RC. (2013) Spontaneous cystogenesis in vitro of a Brazilian strain of Toxoplasma gondii. Parasitol Int. 62(2):181-8. doi: 10.1016/j.parint.2012.12.003.

Paredes-Santos TC, Martins-Duarte ES, de Souza W, Attias M, Vommaro RC. (2018) Toxoplasma gondii reorganizes the host cell architecture during spontaneous cyst formation in vitro. Parasitology. 145(8):1027-1038. doi: 10.1017/S0031182017002050.

Phan L, Kasza K, Jalbrzikowski J, Noble AG, Latkany P, Kuo A, et al. (2008) Longitudinal study of new eye lesions in children with toxoplasmosis who were not treated during the first year of life. Am J Ophthalmol. 146(3).

1365 Plouffe D, Brinker A, McNamara C, Henson K, Kato N, Kuhen K, Nagle A, et al (2008) In silico
1366 activity profiling reveals the mechanism of action of antimalarials discovered in a high-throughput
1367 screen. Proc Natl Acad Sci U S A. 105:9059–9064.
1368
1369 Pybus BS, Marcsisin SR, Jin X, Deye G, Sousa JC, Li Q, et al (2013) The metabolism of
1370 primaquine to its active metabolite is dependent on CYP 2D6. Malaria J. 12:212. doi:
1371 10.1186/1475-2875-12-212.
1372
1373 St Jean PL, Xue Z, Carter N, Koh GC, Duparc S, Taylor M, et al (2016) Tafenoquine treatment of
1374 Plasmodium vivax malaria: suggestive evidence that CYP2D6 reduced metabolism is not
1375 associated with relapse in the Phase 2b DETECTIVE trial Malar J 15:97 DOI 10.1186/s12936-
1376 016-1145-5
1377
1378 Su G, Morris JH, Demchak B, Bader GD. (2014) Biological network exploration with Cytoscape
1379 3. Current protocols in bioinformatics.; 47:8 13 1-24. doi: 10.1002/0471250953.bi0813s47.
1380
1381 Subramanian A, Tamayo P, Mootha VK, Mukherjee S, Ebert BL, Gillette MA, et al. (2005) Gene
1382 set enrichment analysis: a knowledge-based approach for interpreting genome-wide expression
1383 profiles. Proceedings of the National Academy of Sciences of the United States of America.
1384 102(43):15545-50. doi: 10.1073/pnas.0506580102.
1385
1386 Torgerson PR, Mastroiacovo P. (2013) The global burden of congenital toxoplasmosis: a
1387 systematic review. Bull World Health Organ. 91(7):501-8. doi: 10.2471/BLT.12.111732.
1388
1389 Trager, W. & Jensen, J.B., (2005). Human malaria parasites in continuous culture. 1976. The
1390 Journal of parasitology, 91(3), pp.484–486.
1391
1392 Vercesi AE, Rodrigues CO, Uyemura SA, Zhong L, Moreno SNJ. (1998) Respiration and
1393 Oxidative Phosphorylation in the Apicomplexan Parasite Toxoplasma gondii. J. Biol. Chem.
1394 273:31040
1395
1396 Vidigal PVT, Santos DVV, Castro FC, Couto JC de F, Vitor RW de A, Brasileiro Filho G. (2002)
1397 Prenatal toxoplasmosis diagnosis from amniotic fluid by PCR. Rev Soc Bras Med Trop 35(1):1–
1398 6.
1399
1400 Wallon M, Peyron F, Cornu C, Vinault S, Abrahamowicz M, Kopp CB, et al (2013). Congenital
1401 toxoplasma infection: monthly prenatal screening decreases transmission rate and improves
1402 clinical outcome at age 3 years. Clin Infect Dis. 56(9):1223-31. doi: 10.1093/cid/cit032.
1403
1404 Walton NM, Sutter BM, Chen HX, Chang LJ, Roper SN, Scheffler B, et al. (2006) Derivation and
1405 large-scale expansion of multipotent astroglial neural progenitors from adult human brain.
1406 Development. 133(18):3671-81. doi: 10.1242/dev.02541.
1407
1408 Watts E, Zhao Y, Dhara A, Eller B, Patwardhan A, Sinai AP. (2015) Toxoplasma gondii
1409 Bradyzoites within Tissue Cysts Are Dynamic and Replicating Entities In Vivo. Novel approaches

1410 reveal that Toxoplasma gondii Bradyzoites within Tissue Cysts Are Dynamic and Replicating
1411 Entities In Vivo. MBio. 6(5):e01155-15. doi: 10.1128/mBio.01155-15.
1412
1413 Waxman S, Herbert V. (1969) Mechanism of pyrimethamine-induced megaloblastosis in human
1414 bone marrow. N Engl J Med. 280(24):1316–9.
1415
1416 Zheng SQ, Palovcak E, Armache JP, Verba KA, Cheng Y, Agard DA. (2017) MotionCor2 -
1417 anisotropic correction of beam-induced motion for improved cryo-electron microscopy. Nat
1418 Methods. 14(4): 331–332. oi: 10.1038/nmeth.4193
1419
1420 Zhang, J, Tan, P, Guo, L, Gong, J, Ma, J, Li, J et al. (2016) p53-dependent autophagic. Cryo-EM
1421 of Cellular Machineries. PNAS U.S.A. 2016;113 (41):11519-11524. 10.1073/pnas.1707102114.
1422
1423
1424 Conflict of Interest Statement: RM, MM. CWF, CWR, KE, MH, QQLand HL are inventors on an
1425 International patent application PCT/US2016/067795 pertinent to the wotk in this study. RM has
1426 completed an unrelated literature review for Sanofi-Pasteur
1427
1428 Citation *McPhillie M, Zhou Y, Hickman M, Gordon J, Weber CR, Qigui Li*[3], *Lee P,*
1429 *Amporndana, K, Johnson R, Darby H, Woods S, Li SZ-h, . Priestley RS, Ristroph K, Biering S,*
1430 *El Bissati K, Hwang S*[+], *Esaa Hakim F , Dovgin S, Lykins J, Roberts L , Hargrave K , Hua C,*
1431 *Sinaii AP, . Muench SP, Dubey JP, Prud'homme R, Lorenzi H*[1], *GA Biagini*[7], *. Moreno SN, Roberts*
1432 *CW, Atonyuk S, Fishwick CW, McLeod R*
1433
1434
1435 **FIGURE LEGENDS**

1436 **Figure 1. Characteristics and effects of compounds on inhibition of *T.gondii* replication and**
1437 **enzyme activity, and Structure Activity Relationship analysis. A. Cytochrome b/c inhibitor**
1438 **code, Chem Draw structure, solubility in PBS 7.4, toxicity against HFF, predicted half-life,**
1439 **and inhibitory effect of compounds on RH strain tachyzoites and EGS strain bradyzoites *in***
1440 ***vitro*. and saffarine O assay enzyme activity.** PBS Sol/Toxicity pH7.4 refers to solubility of the
1441 compound in Phosphate Bufferred Saline (PBS) at pH7.4. Toxicity refers to the highest
1442 concentration tested that does not show toxicity to Human Foreskin Fibroblast (HFF) in tissue
1443 culture in WST assay; T1/2 (H) refers to the predicted half-life in human liver microsomes; T1/2

1444 (M) refers to the predicted half-life in mouse liver microsomes. Tachy/Brady IC50 was determined
1445 in studies in which cultures of parasites in HFF were treated with varying concentrations of the
1446 compound and there was 50% inhibition of the replication (number) of parasites. Parasites were
1447 RH-YFP expressing tachyzoites (Tachy) and EGS (Brady) strains. Studies of effects of inhibitors
1448 on HFF or on *T.gondii* tachyzoites were performed with triplicate wells in at least 2 biological
1449 replicate experiments**.** Studies of effects on bradyzoites were performed at least twice in at least 2
1450 biological replicate experiments**.** Compounds with much less inhibition of mammalian than *T.*
1451 *gondii* cytochrome *bc* in the saffarine enzyme assay (indicated by **) provide potential to further
1452 develop compounds, if unanticipated toxicity occurs from JAG21. **B. Structure Activity**
1453 **Relationship analysis (SAR).** The effects of changing R1 as 7-Et, 7-Me, 6-CF_3, or 6-Me on
1454 activity against *T.gondii* RH strain tachyzoites, solubility, and stability were compared in the SAR.
1455 Colour Key in B: *Activity*: Green <50 nM, Red > 1 μM; *Solubility* in 100 mM Phosphate Buffer
1456 (pH 7.4): Amber>10 μM, Red <10 μM; *Metabolic Stability*: Green >120 mins, Amber 60-120mins,
1457 red < 60 mins. SAR panel displays only representative structures and trends within the JAG
1458 compound series. JAG21 (blue font) is highly active, has the longest predicted half-life for humans
1459 of initial compounds tested (green), combined with improved solubility, no hERG liability, and
1460 predicted capacity to cross the blood brain barrier (BBB). Definitions of ADMET terminology are
1461 in the Materials and Methods. In summary, in the SAR overall, nitrogen atoms not tolerated in aryl
1462 ring (C) and the 4-position was optimal for phenol substituent
1463

1464 **Figure 2**. **JA21 is potent *in vitro* against *T. gondii*, tachyzoites and bradyzoites, and multiple**
1465 **drug resistant strains of *P. falciparum* A. JAG is effective Against RH-YFP tachyzoites, and**
1466 **does not harm human cells.** Potent effect of JAG 50 is also shown. A representative experiment

1467 is shown. N=triplicate wells in at least 2 biological replicate experiments. Relative fluorescence
1468 units are shown on vertical axis, where decrease in fluorescence compared to diluent DMSO in
1469 media control indicates parasite inhibition. Horizontal axis indicates different treatment
1470 conditions: This shows results of testing of fibroblasts in media (HFF), DMS0 control, positive
1471 control pyrimethamine (P) and sulfadiazine(S), and concentrations of JAG21 and JAG50 utilized.
1472 Differences were not statistically significant in the cytotoxicity assay (data not shown),. **B.**
1473 **JAG21 is effective against EGS bradyzoites.** Effect of JAG21 in reducing bradyzoites in HFF
1474 by parasite strain EGS. HFF were infected by EGS and treated with JAG21 at concentrations
1475 indicated. Slides were stained with Dolichos Biflorus Agglutinin conjugated with FITC (which
1476 stains the cyst wall) and DAPI, and observed with fluorescence microscopy. The red arrows point
1477 to the Dolichos enclosed organisms formed in tissue culture. These were eliminated with treatment
1478 with JAG21. This experiment was performed >4 times. These experiments were performed with 3
1479 different observers reviewing slides at the microscope quantitating fields for each condition.
1480 Slides were also scanned and the scans of the slides were reviewed so all fields in the entire slide
1481 were noted to be consistent . **C. Synergy of JAG21 and atovaquone against Rh-YFP**
1482 **tachyzoites *in vitro***. Isobologram comparing JAG21, atovoquone, and JAG21 plus atovaquone
1483 demonstrates synergy. **D. THQs effective against drug resistant *P. falciparum*.** Dose-response
1484 phenotypes of a panel of *P. falciparum* parasite lines. IC50 values were calculated using whole-cell SYBR
1485 Green assay and listed as mean +/- standard deviation of three biological replicates, each with triplicate
1486 measurements. The D6 strain is a drug sensitive strain from Sierra Leone, the TM91-C235 strain is a multi-
1487 drug resistant strain from Thailand, the W2 strain is a chloroquine resistant strain from Thailand, and the
1488 C2B strain is a multi-drug resistant strain with resistance against atovaquone. **E. Solubility and Stability**
1489 **in human and mouse liver microsomes comparing MJM 170, JAG21 and JAG50.** Performed by Chem

1490 Partners. **F. JAG21 CYP450 Inhibition, CACO-2, hERG, PPB, BBB (MDCK-MDK1 efflux analyses.**
1491 These were performed by Chem Partners and are as defined in the Materials and Methods..
1492
1493 Figure 3. Effect of JAG21, and other THQ compounds on mitochondrial functions of. *T.gondii*
1494 and. *P. falciparum* and HFF-hTERT A. Maximum mitochondrial membrane depolarization of
1495 JAG21, JAG39, JAG46, JAG47, JAG50 and Atovaquone (4 μM) and FCCP (5 μM). Digitonin
1496 was added where indicated by the arrow to permeabilize cells and permit a necessary mitochondrial
1497 substrate (Succinate) to reach intracellular organelles. The addition of the indicated compounds is
1498 shown by the second arrow. B. Quantification of the depolarization shown in A. The relative
1499 depolarization of each compound was normalized to the depolarization by FCCP which was
1500 considered 100% depolarization. C. Effect of various concentrations of JAG21 and Atovaquone
1501 on the mitochondrial membrane potential measured as in A. The first arrow indicates digitonin
1502 addition and the second arrow indicates the addition of compounds at the specified concentration.
1503 D. Quantification of the depolarization measured in C. The relative depolarization of each
1504 compound was normalized to the depolarization by FCCP (100%). E. Mitochondrial membrane
1505 depolarization of HFF-hTERT in suspension by JAG21 and atovaquone. The first arrow indicated
1506 the addition of digitonin, and the second arrow indicates addition of the indicated compounds at
1507 the indicated concentration. F. Quantification of the depolarization measured in E. The relative
1508 depolarization of each compound was normalized with the depolarization by FCCP, which was
1509 considered 100%. B, D, E X+/-S.D., N=3 independent experiments. Statistical analysis (unpaired
1510 student t test) was performed using GraphPad Prism 8.0 (GraphPad Software, Inc., San Diego,
1511 CA). **. $P < 0.01$. ***. $P < 0.001$. g. JAG21, JAG99 and MJM210 (1 μM) inhibited *P. falciparum*
1512 cytochrome c reduction. Vehicle (DMSO)/atovaquone (1 μM) were negative/positive controls,
1513 1290 respectively. X+/-S.D., N=4 independent experiments.

1514

1515 **Figure 4. Binding studies of JAG021 to bovine bc1**. **A. Bovine Cytbc1 activity assays** showing
1516 36% and 63% inhibition at 0.1 and 1μM concentration of JAG021, respectively. N= at least 2
1517 biological replicate experiments with similar results. **B.** The Cytbc1 structure presented in cartoon
1518 style with clear omit (Fo-Fc) electron density map for the bound JAG021 compound only in the
1519 Q_i site showing selectivity within the binding pocket. Qi and Qo sites are marked by
1520 black ellipsoids. **C.** The bound JAG021 compound (orange) within the Qi site with
1521 corresponding (2Fo-Fc) electron density map contoured at 1 σ level as grey mesh. The residues
1522 which make close interactions with the bound inhibitor are shown in stick format and labelled.
1523 **D.** 2D pharmacophore analysis of JAG021 binding pocket produced using Ligplot+ LS-2011.
1524 Hydrophobic interactions are shown as red spikes, hydrogen bond with Ser35 is shown by green
1525 dashes. **E.** Cryo-EM derived structure of the Cytbc1 bound JAG021 structure with corresponding
1526 density map contoured at 3 σ level suggesting two different positions for the head group
1527 represented by two regions of density shown as yellow mesh. The Cytbc1 structure bound to the
1528 pyridone GSK932121 (PDB:4D6U) (**F**) and quinolone MJM170 (PDB:5NMI) **(G)** in the Q_i site.
1529 Haem and compounds are shown as colored sticks, Fe ion as orange sphere and hydrogen bonding
1530 as black lines. Hydrogen bonding with Ser35 is shown as black dashes.

1531

1532 **Figure 5** . **JAG21 is a mature lead that protects against *T. gondii* and *P.berghei in vivo*. A.**
1533 **JAG21 treatment for 14 days protects against *T.gondii* tachyzoites *in vivo*.** Tachyzoite
1534 challenge with Prugneaud luciferase parasites imaged with leuciferin using IVIS demonstrates that
1535 treatment with JAG21 eliminates leuciferase expressing parasites and leads to 100% survival of
1536 JAG21 treated infected mice. No cysts were found in brains of mice at 30 days after infection

1537 when they have been treated with JAG21 for the first 14 days after infection. There were 2
1538 biological replicate experiments with 5 mice per group with similar results**. B. JAG21 and JAG21**
1539 **plus tafenoquine markedly reduce Me49 strain brain cyst numbers *in vivo* in Balb/C mice at**
1540 **30 days after infection.** Parasites were quantitated by scanning the entire immunoperoxidase
1541 stained slide in an automated manner and by two observers blinded to the experimental treatment
1542 using microscopic evaluation**.** In each of two experiments, the numbers of mice per group were
1543 as follows: Experiment 1 had 4 diluent controls, 5 JAG21, 4 JAG21/Tafenoquine treated mice;
1544 and Experiment 2 had 5 diluent controls, 5 JAG21, 3 JAG21/Tafenoquine treated
1545 mice. Immunoperoxidase staining was performed. Parasite burden was quantitated using a
1546 positive pixel count algorithm of Aperio ImageScope software. Positive pixels were normalized to
1547 tissue area (mm^2). Quantification was by counting positive pixels per square area. The entire brain
1548 in one section was scanned for each mouse. The parasite burden was quantitated as units of
1549 positive pixels per mm^2. The average +/- S.E.M. numbers of mm^2 per slide quantitated
1550 was 30.2+/-1.6 mm^2 per mouse for this quantification. Each high power field of view shown in
1551 **C** is approximately 0.02 mm^2 per field of view. A representative single experiment is presented
1552 and the data from the two experiments analyzed together also demonstrated significant differences
1553 between the untreatated and treated groups ($p<0.01$; Supplemental **Fig. S1**.). **C. Microscopic**
1554 **evaluation of the slides** reveal effect of JAG21 and JAG21 plus tafenoquine having the same
1555 pattern as the automated quantitation of immunoperoxidase stained material. There are usual
1556 appearing cysts in the DMSO control untreated mice as shown in the top panels, and rare cysts in
1557 the treated mice with most of the brown material appearing amorphous (bottom panels). **D. JAG21**
1558 **nanoformulation dosages administered to *P.berghei* infected C57Bl6/albino mice compared**
1559 **with vehicle control.** Design of single dose and 3 day dose experiments. **E. JAG21**

1560 **nanoformulation cures *P. berghei* sporozoites(c), blood(d) and liver stages(e) with oral**
1561 **administration of a single dose of 2.5mg/kg or 3 doses at 0.625mg/kg.** Single dose causal
1562 prophylaxis in 5 C57BL/6 albino mice at 2.5 mpk dosed on day 0, 1 hour after intravenous
1563 administration of 10,000 *P. berghei* sporozoites. Shown is 3 dose causal prophylaxis treatment in
1564 5 C57BL/6 albino mice at 0.625 mpk dosed on days -1, 0, and +1. Representative figure showing
1565 survival, luminescence and parasitemia quantitated by flow cytometry for 5 mg/kg.
1566
1567 **Figure 6. *T. gondii* ΔRPS13 transcriptome during Primary Human Brain Neuronal Stem**
1568 **Cell (NSC) infection and *in-vivo* susceptibility to JAG21 and TAF treatment are reminiscent**
1569 **of literature findings with malaria hypnozoites. A**, *P. cynomolgi-T. gondii* best reciprocal match
1570 genes significantly upregulated (red) or downregulated (blue) in *P. cynomolgi* hypnozoites
1571 compared to liver-schizont stage and in ΔRPS13 after downregulation of *rps13* gene expression
1572 (p-value ≤ 0.05, FDR ≤ 0.2). **B**, Gene-set enrichment analysis of ΔRPS13 +/-Tc. Blue and red
1573 nodes denote gene-sets enriched in presence or absence of Tc respectively. Node diameters are
1574 proportional to number of genes belonging to corresponding gene-sets. Edge thickness is
1575 proportional to number of genes shared between connected nodes. **C**, Survival rate of mice
1576 infected with 100,000 ΔRPS13 followed by treatment with diluent, JAG21, tafenoquine (TAF) or
1577 the two together (JAG21/TAF). Then tetracycline was added at 14 days. The combination of the
1578 two compounds resulted in improved time of survival (p<0.03, Experiment 1;p=0.08 Experiment
1579 2, p=0.002 Experiment 1+2). The full data are presented in the box below the image in **Fig 6C. In**
1580 **6C,** Rx refers to treatment of mice with diluent (DMSO), Tafenoquine (TAF), or JAG21, or JAG21
1581 and TAF. ΔRPS13 is referred to as RhRPS13Δ in the title of the box **in Fig 6C**. In Supplemental
1582 **Fig.S2**, histological preparations that are immunoperoxidase stained for *T gondii* antigens from a

1583 pilot study were prepared (**Supplemental Fig. S2**). These are images, in **Fig S2** of liver and spleen
1584 from IFN γ receptor knock out mice without treatment on days 7 and 14 after infection. In those
1585 mice without any treatment there was amorphous brown immunoperoxidase stained material in
1586 **Fig S2 A**. When tetracycline (aTet) was administered on day 14 after infection in drinking water
1587 on day 14 and tissues obtained and immunostained for *T. gondii* antigens from mice that died or
1588 became very ill, organisms clearly recognizable could be seen (Supplemental **Fig S2B-E**). Design
1589 of the treatment experiment with control DMSO diluent, JAG21 alone, Tafenoquine alone (TAF)
1590 or the two together (JAG/TAF) with full data for each of the groups and with the composite
1591 analysis from replicate experiments, including numbers of mice, are shown in supplemental **Fig.**
1592 **S2C, D.** **Fig S2 C, D** shows prolongation of survival time, but there is not durable protection
1593 against ΔRPS13 in these immune compromised mice treated with JAG21/TAF as described. This
1594 is summarized in **C** to demonstrate early prolongation of survival time with the detailed data in
1595 **Fig S2. D. Gene ontology enrichment analysis of ΔRPS13 +/-Tc.** Node and edge conventions
1596 are the same as in **B. There were at least 2 biologic replicates of each experiment.**
1597

1598 **Figure 7. Oral nanoformulation of JAG21 potently protects against 2000 highly virulent RH**
1599 **strain tachyzoites given intraperitoneally.** **A.** Folllowing sonication produces nanoparticles of
1600 ~2.86microM. **B.** Single oral dose of 10mg/kg reduced intraperitoneal tachyzoites measured by
1601 RH YFP expression and counting with hematocytometer($p<0.03$),, **C.** Three daily 10mg/kg doses
1602 markedly and significantly reduces intraperitoneal parasite burden measured as fluorescence and
1603 by hematocytometer on the fifth day($p<0.001$).No compound was administered after the third day.
1604 N=at least 2 biological replicate experiments with 5 mice per group with similar results.

Figure 1.JPEG

A Code	Structure	PBS Sol /Toxicity* pH7.4 μM	$T_{1/2}$ (H)	$T_{1/2}$ (M)	Tachy/ Brady IC_{50} μM
JAG021	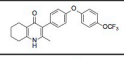	7.07/*	>7 days	101.09	0.12/2
JAG022	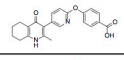	ND/5	ND	ND	7.6/ ND
JAG046	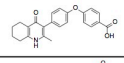	ND/5	ND	ND	>10/ND
JAG047	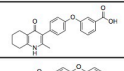	ND/5	ND	ND	>10/ND
JAG050	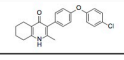	16.41/*	99.04	68.55	0.085/2
JAG062	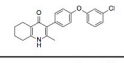	0.33/*	135.3	12.42	0.016/1
JAG069	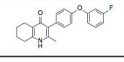	0.5/*	201.98	17.38	0.03/1
JAG084	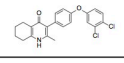	0.68/*	ND	63.1	0.055/1
JAG204	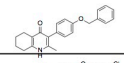	ND/5	ND	ND	0.02/1
JAG208	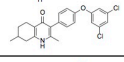	ND/5	ND	ND	0.02/1
JAG058	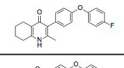	2.38/*	263.1	39.17	0.04/1
JAG063	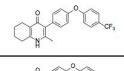	0.45/*	536.6	126.96	0.2/ND
JAG023	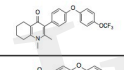	ND/5	ND	ND	0.8/ND
JAG077	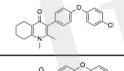	ND/5	ND	ND	0.4/ND
AS006**	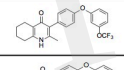	0.55/*	ND	25.88	0.06/1
AS012**	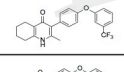	2.19/*	ND	30.05	0.26/ND
AS021	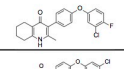	2/*	ND	41.09	0.065/1
AS034	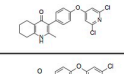	5.05/*	ND	24.93	0.28/ND
AS022	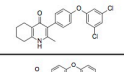	6.25/*	ND	28.62	0.03/1
JAG091	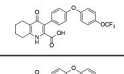	ND/5	ND	ND	>10/ND
JAG092	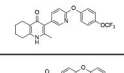	ND/5	ND	ND	1/ ND
JAG095	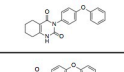	ND/5	ND	ND	>10/ND
JAG099	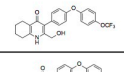	4.05/*	ND	ND	0.38/ND
AS032**	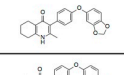	ND/5	ND	ND	0.2/ND
AS033	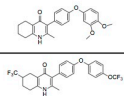	ND/5	ND	ND	ND
JAG100**	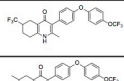	ND/5	ND	ND	>10/ND
JAG106	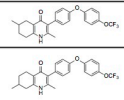	ND/5	ND	ND	2.5/ND
JAG107	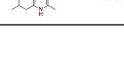	0.03	ND	111.93	0.05/ND

Code	Structure	PBS Sol /Toxicity* pH7.4 μM	$T_{1/2}$ (H)	$T_{1/2}$ (M)	Tachy/Brady IC_{50} μM
JAG121"**	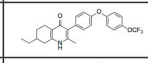	0.16	ND	63.28	0.055/ND
JAG162**	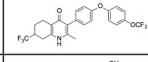	0.02	ND	144.43	0.3/ND
JAG094	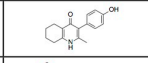	ND/5	ND	ND	1/ND
JAG171	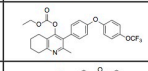	ND/5	ND	ND	0.1/ND
JAG174	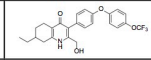	ND/5	ND	ND	0.38/ND
JAG187**	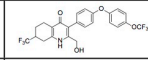	ND/5	ND	ND	2/ND
JAG193	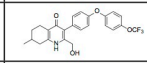	ND/5	ND	ND	0.05/ND
NP032	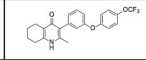	ND/5	ND	ND	0.2/ND
NP034	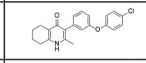	ND/5	ND	ND	0.08/ND
NP035	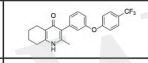	ND/5	ND	ND	0.65/ND
JAG199	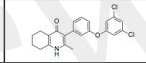	ND/5	ND	ND	0.2/ND
JAG200	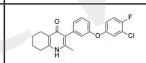	ND/5	ND	ND	0.06/ND
MJM170	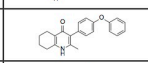	1.97/*	146.33	20.97	0.03/4
ELQ271	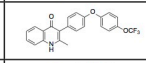	0.15/*	171.93	448.13	0.03/5
JAG039	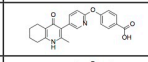	ND/5	ND	ND	7.6/ND
JAG129	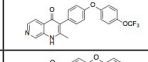	5.12	N.D.	∞	0.085/ND
JAG006	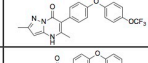	ND/5	ND	ND	5/>10
JAG013	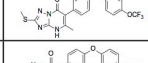	ND/5	ND	ND	10/ND
JAG014	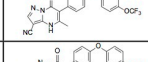	ND/5	ND	ND	>10/ ND
JAG015	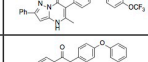	ND/5	ND	ND	10/ND
MJM129	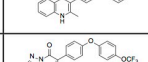	ND/5	ND	ND	0.05/>10
MJM136	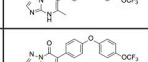	ND/5	ND	ND	3.1/ >10
MJM141	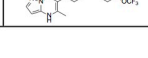	0.94/*	278.33	ND	8.2/10

B

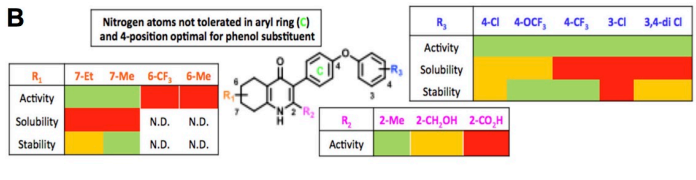

Figure 2.TIF

A

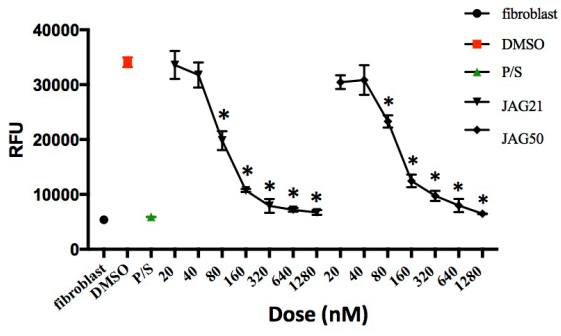

B

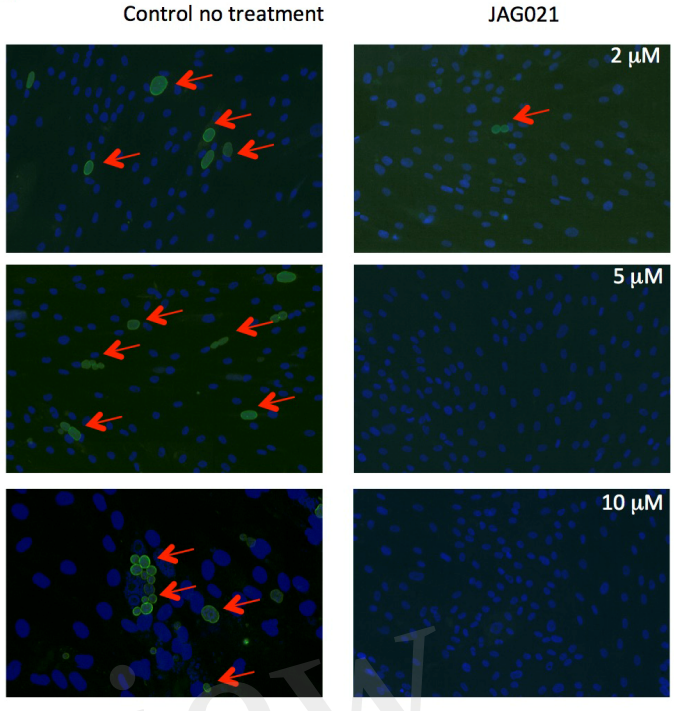

C

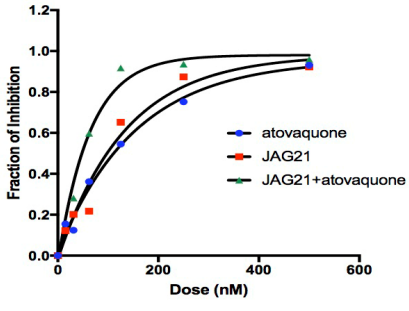

D

Compound ID	SYBR Green D6 IC50 (µM)	SYBR D6 R^2	SYBR Green C235 IC50 (µM)	SYBR TM91C235 R^2	SYBR Green W2 IC50 (µM)	SYBR W2 R^2	SYBR Green C2B IC50 (µM)	SYBR C2B R^2
JAG021	0.01435	0.9572	0.06164	0.9706	0.05518	0.9727	0.04042	0.9847
JAG050	0.04664	0.9138	0.06913	0.9562	0.03136	0.9693	0.03635	0.9427
JAG047	3.746	0.9738	12.56	0.9218	9.072	0.9358	7.781	0.9575
JAG039	9.595	0.9532	>20	N/A	>20	N/A	>20	N/A
JAG046	6.716	0.9844	>20	N/A	>20	N/A	>20	N/A
JAG006	0.29	0.90	0.88	0.92	2.46	0.92	1.66	0.94
RG38	2.884	0.8936	13.66	0.8338	9.245	0.7954	>20	N/A

E

Compound ID	Solubility (pH 7.4) (µM)	Human liver microsomes (min)	Mouse liver microsomes (min)
MJM170	1.97	146.33	20.97
JAG021	7.07	∞	101.09
JAG050	16.41	99.04	68.55

F

JAG21 **CYP 450** inhibition, IC50 >10µM 4/5 isoforms; 4.0µM (2C9) ; **CACO-2**(P_{app}A-B)cm/s >10x10^{-6} ; **Herg IC50**=22µM; **PPB(human)**=99.9; **BBB**= **MDCK-MDK1 system**, exhibits high permeability (P_{app} >10 x10^{-6} cm/s) and **low efflux** (efflux ratio <1.5)

Figure 3.JPEG

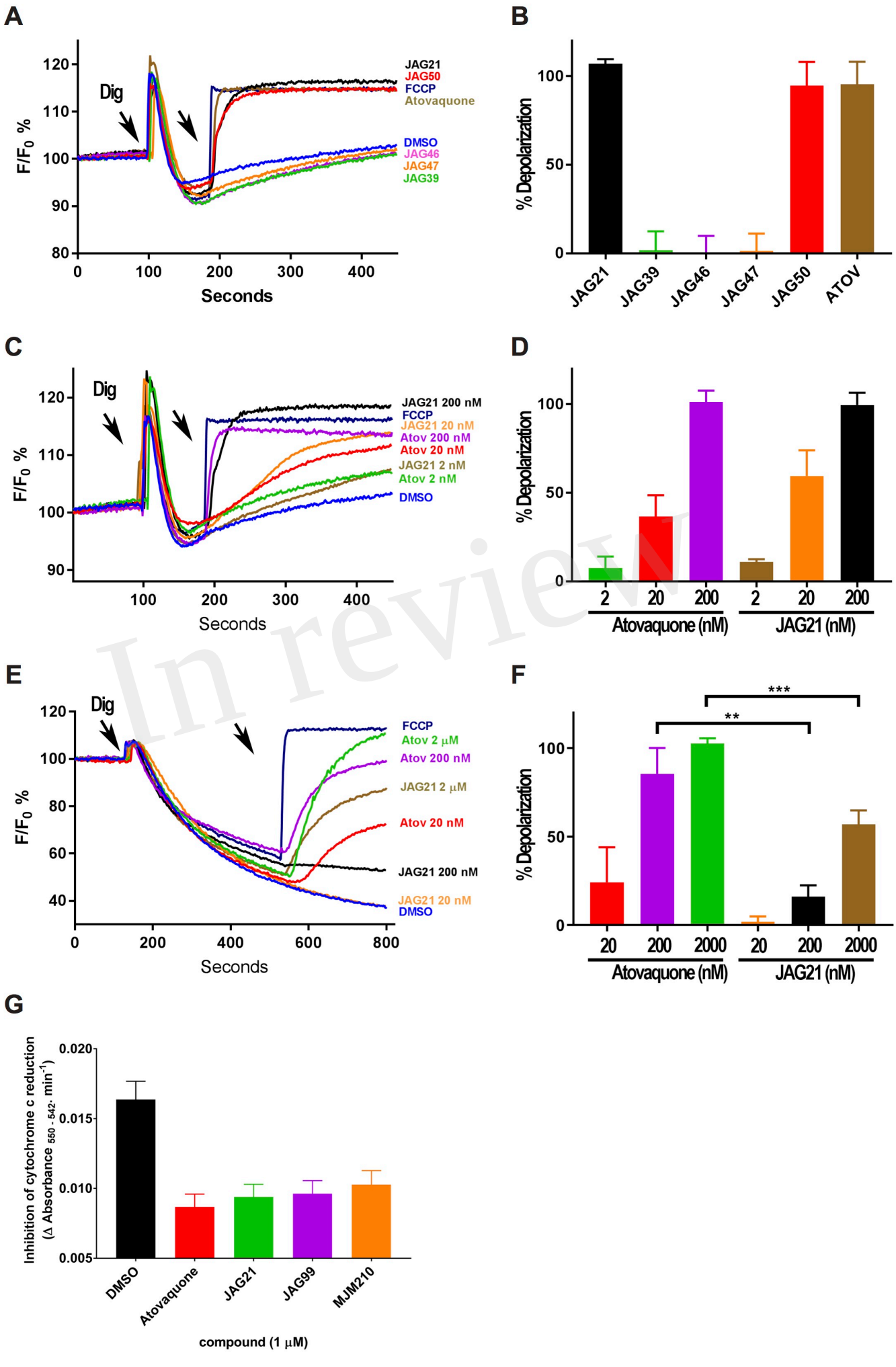

Figure 4.JPEG

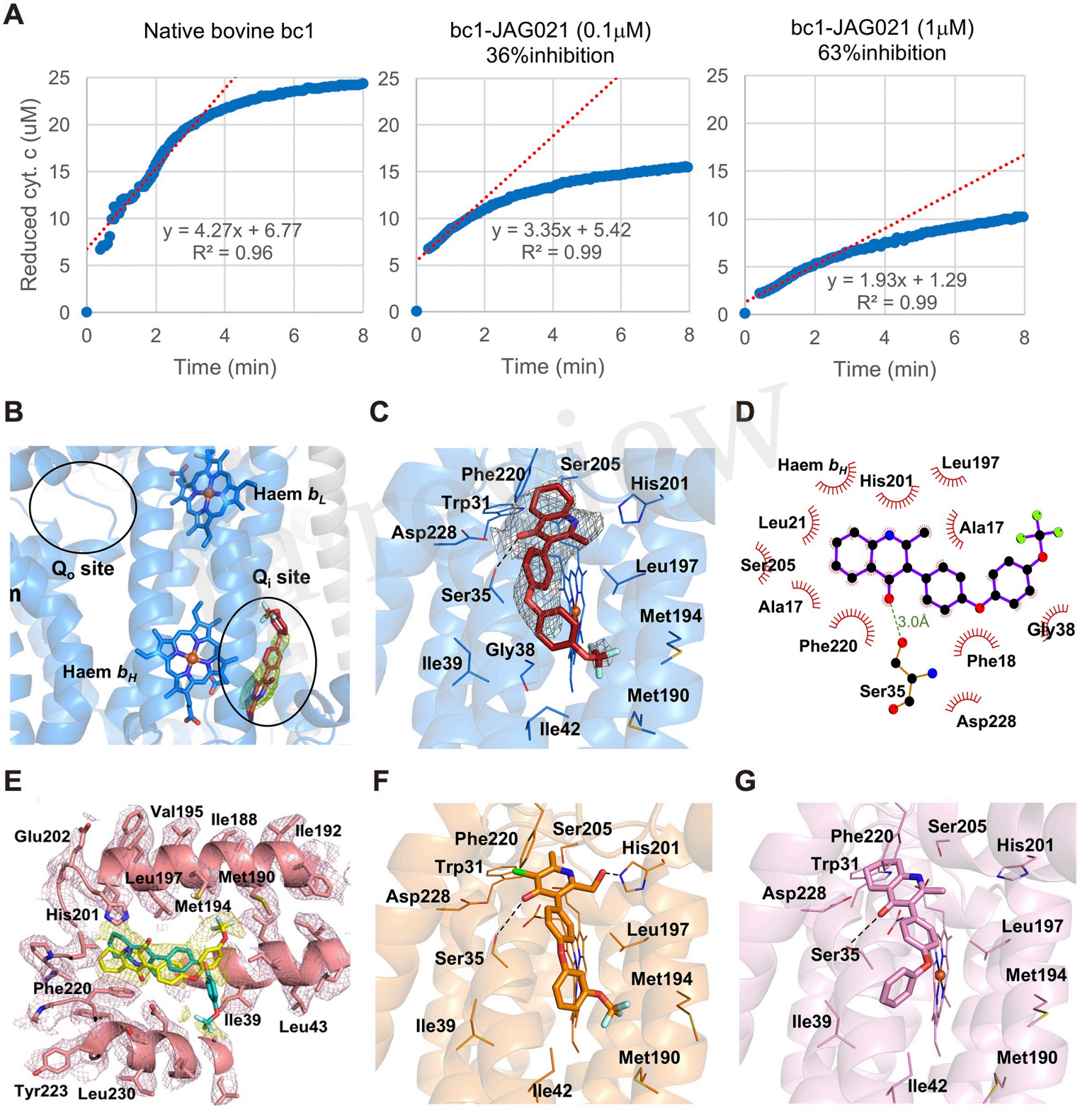

Figure 5.JPEG

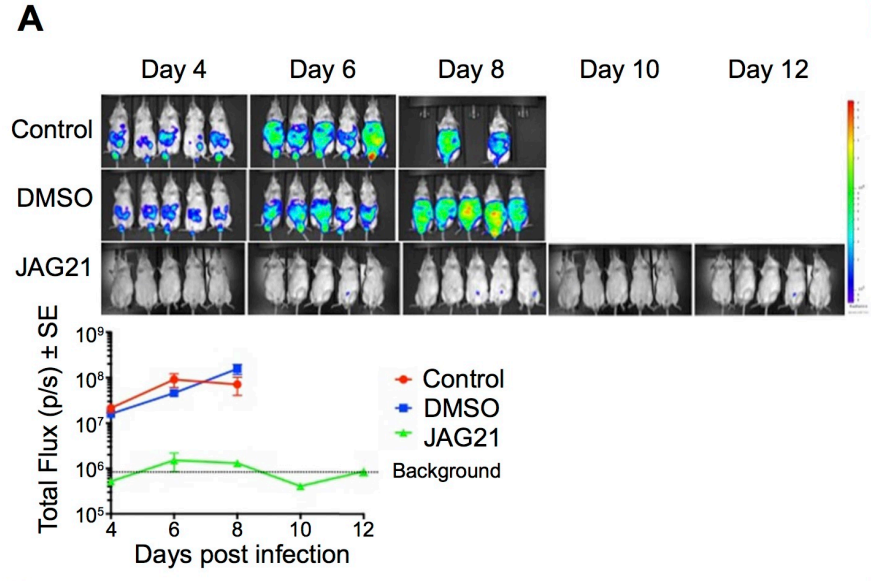

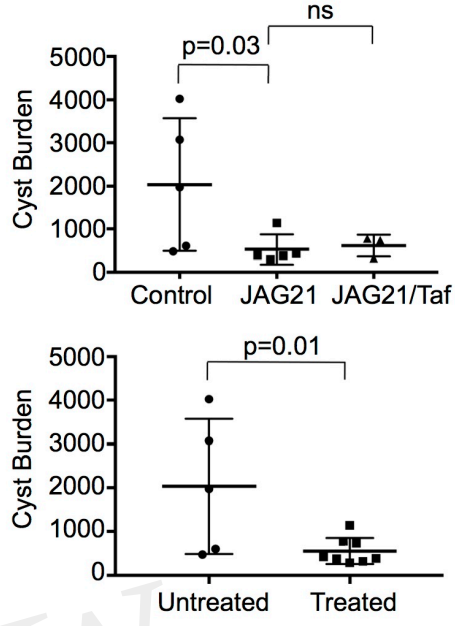

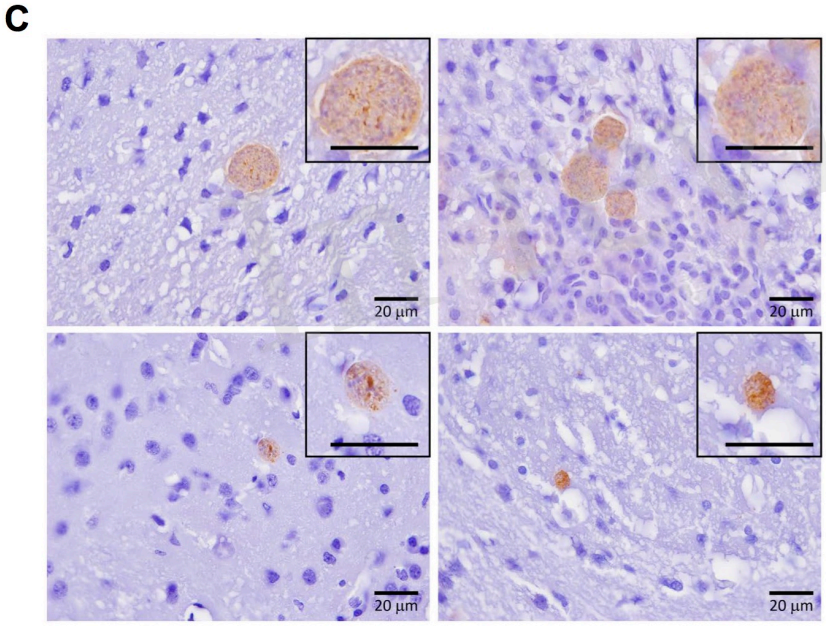

D

In vivo efficacy P.berghei model	JAG21			
P.O. (3 doses) -D1, D0, D1	10 mg/kg	5 mg/kg	2.5 mg/kg	0.625 mg/kg
IVIS @ 72h	0	0	0	0
Mean Survival Days	30	30	30	30
	ED90 < 1.25 mg/kg for 3 daily doses			

In vivo efficacy P.berghei model	JAG21			
P.O. (single dose)	1.25 mg/kg -D1	2.5 mg/kg -D1	1.25 mg/kg D0	2.5 mg/kg D0
IVIS @ 72 h	> $10x10^6$	> $10x10^6$	0	0
Mean Survival Days	8	15	>17	30
	ED90 < 2.5 mg/kg single dose			

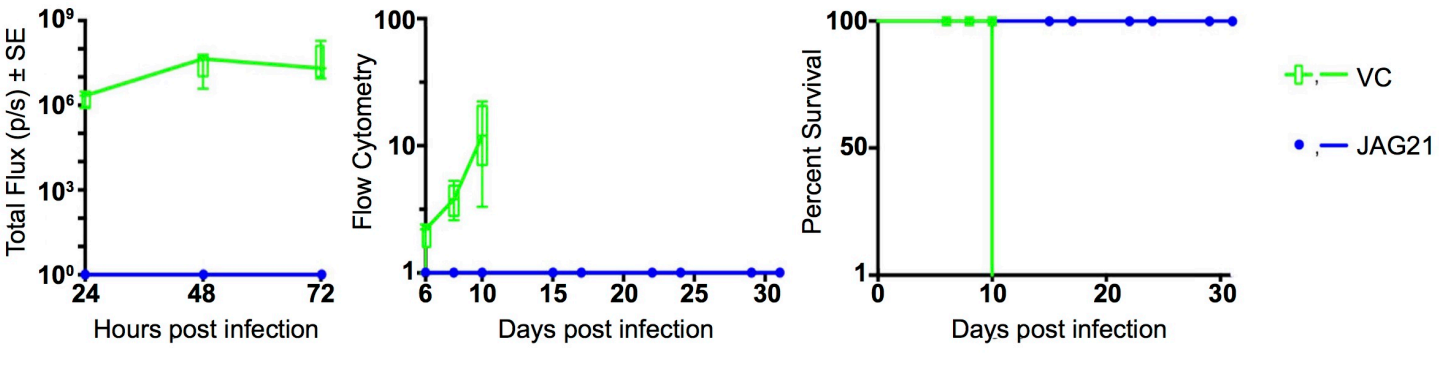

Figure 6.TIF

A

Description	*P. cymonolgi* Gene_ID	*P. cymonolgi*	*T. gondii*	*T. gondii* Gene_ID	Description
erythrocyte binding protein	PCYB_063210			TGME49_310170	hypothetical protein
hypothetical protein	PCYB_061360			TGME49_261960	hypothetical protein
hypothetical protein	PCYB_073220			TGME49_268240	hypothetical protein
hypothetical protein	PCYB_091490			TGME49_234410	small conductance mechanosensitive ion channel
serine/threonine protein kinase	PCYB_021650			TGME49_311510	eIF2 kinase IF2K-B
hypothetical protein	PCYB_073210			TGME49_292330	hypothetical protein
protein kinase domain containing protein	PCYB_032180			TGME49_268010	hypothetical protein
hypothetical protein	PCYB_145980			TGME49_276180	histone acetyltransferase TAF1/250
TBC domain containing protein	PCYB_071500			TGME49_203910	TBC domain-containing protein
hypothetical protein	PCYB_127100			TGME49_206550	hypothetical protein
hypothetical protein	PCYB_093980			TGME49_273860	hypothetical protein
hypothetical protein	PCYB_111820			TGME49_293820	calpain family cysteine protease, putative
eukaryotic initiation factor	PCYB_091430			TGME49_269180	MIF4G domain-containing protein
hypothetical protein	PCYB_141480			TGME49_231480	GCN1, putative
Sec20-like protein	PCYB_142610			TGME49_217780	Sec20 protein
hypothetical protein	PCYB_052770			TGME49_249970	hypothetical protein
DEAD/DEAH box helicase	PCYB_071120			TGME49_294350	DEAD/DEAH box helicase, putaitve
hypothetical protein	PCYB_091600			TGME49_277080	microneme protein MIC5
origin recognition subunit	PCYB_011270			TGME49_245570	origin recognition complex subunit 2 protein
hypothetical protein	PCYB_113090			TGME49_261230	ankyrin repeat-containing protein
hypothetical protein	PCYB_073640			TGME49_309170	TAF7-like RNA polymerase II TAF7L
hypothetical protein	PCYB_063170			TGME49_258820	hypothetical protein
hypothetical protein	PCYB_143620			TGME49_229740	hypothetical protein
40S ribosomal protein S13	PCYB_112180			TGME49_270380	ribosomal protein RPS13
20S proteasome subunit alpha type 2	PCYB_114800			TGME49_287210	proteasome subunit alpha2, putative
hypothetical protein	PCYB_143610			TGME49_242890	hypothetical protein
pre-mRNA splicing factor	PCYB_031320			TGME49_231970	pre-mRNA processing splicing factor PRP8
4-methyl-5(B-hydroxyethyl)-thiazol monophosph. biosynth.	PCYB_113050			TGME49_214290	DJ-1 family protein
5'-3' exonuclease N-terminal resolvase-like domain	PCYB_042630			TGME49_284010	5'-3' exonuclease, N-terminal resolvase family
multidrug resistance protein 2	PCYB_126720			TGME49_249820	ATP-binding cassette sub-family B member 5
2-oxoglutarate dehydrogenase E1 comp. mitoch. prec.	PCYB_052050			TGME49_244200	2-oxoglutarate dehydrogenase E1 component
protein disulfide isomerase	PCYB_051340			TGME49_211680	protein disulfide isomerase
pyruvate dehydrogenase E1 component alpha subunit	PCYB_093050			TGME49_245670	pyruvate dehydrogenase complex subunit PDH-E1∝
hypothetical protein	PCYB_133950			TGME49_291140	CCR4-Not complex component, Not1 protein
hypothetical protein	PCYB_113850			TGME49_313590	hypothetical protein
hypothetical protein	PCYB_146850			TGME49_240910	hypothetical protein
elongation factor 1 alpha	PCYB_112350			TGME49_286420	elongation factor 1-alpha (EF-1-ALPHA), putative
cytochrome c oxidase subunit	PCYB_073540			TGME49_209260	cytochrome c oxidase subunit, putative
ubiquinol-cytochrome c reductase	PCYB_082210			TGME49_288750	ubiquinol-cytochrome c reductase
proteasome beta-subunit type 4	PCYB_012310			TGME49_280710	20S proteasome subunit beta 7, putative
DNA polymerase alpha	PCYB_031930			TGME49_217910	DNA polymerase (pol2) superfamily protein
hypothetical protein	PCYB_082250			TGME49_228330	NLI interacting factor family phosphatase
ubiquitin-like protease 1 homolog Ulp1 homolog	PCYB_012530			TGME49_251510	Ulp1 protease family, catalytic domain
hypothetical protein	PCYB_095140			TGME49_224590	DNA-directed RNA polymerase III POLR3C
vacuolar ATP synthetase	PCYB_102260			TGME49_212310	vacuolar ATP synthetase

B

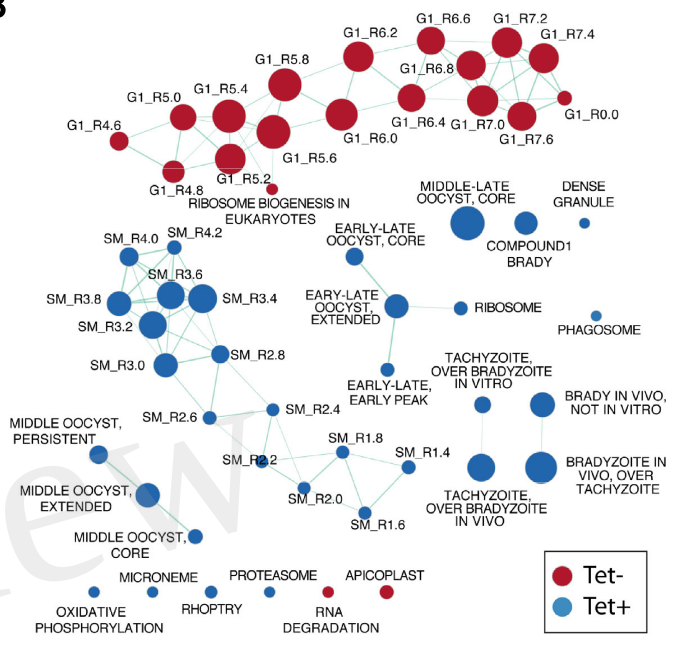

C

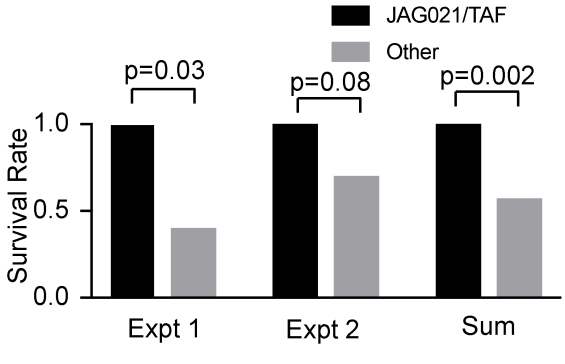

RhRPS13 infection mortality prior to initial JAG21+TAF mortality					
Rx	Single Rx			Sum of Single Rx	Combined Rx
	DMSO	TAF	JAG21	DMSO or TAF or JAG21	JAG21 + TAF
Expt 1	2/5	4/5	3/5	9/15	0/6
Expt 2	3/10	2/5	1/5	6/20	0/9
Total	**5/15**	**6/10**	**4/10**	**15/35**	**0/15**

D

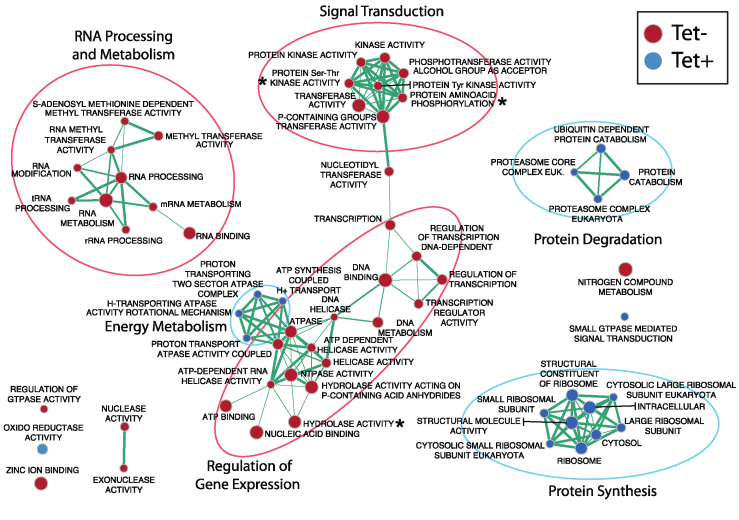

Figure 7.JPEG